

## RESEARCH ARTICLE

# Meteorological conditions leading to a catastrophic, rain-induced landslide in Cameroon in October 2019

Derbetini A. Vondou<sup>1,2</sup>  | Marlon Maranan<sup>2</sup>  | Andreas H. Fink<sup>2</sup>  | Peter Knippertz<sup>2</sup> 

<sup>1</sup>Laboratory for Environmental Modelling and Atmospheric Physics, Department of Physics, University of Yaoundé I, Yaoundé, Cameroon

<sup>2</sup>Institute of Meteorology and Climate Research Troposphere Research, Karlsruhe Institute of Technology, Karlsruhe, Germany

## Correspondence

Derbetini A. Vondou, Laboratory for Environmental Modelling and Atmospheric Physics, Department of Physics, University of Yaoundé I, Yaoundé, Cameroon.

Email: [derbetini@yahoo.fr](mailto:derbetini@yahoo.fr)

## Abstract

After an exceptionally wet October 2019, the city of Bafoussam in the Cameroon Highlands was hit by a devastating landslide on 29 October, resulting in around 50 deaths. This study examines the atmospheric drivers leading up to this fatal event on a submonthly scale. Leveraging long-term station rainfall data from Bafoussam and the nearby city of Dschang, three marked wet spells during October 2019 are identified, the multiday rainfall amounts of which exceed the maximum value within the historical data of the stations. Using ERA5 reanalysis data, favourable conditions in each of these wet spells were created by moist southwesterlies, promoted by transient cyclonic vortices over the eastern Guinea coast. The release of the intense rainfalls is associated with strong moisture flux convergence (MFC), likely through an interaction between the southwesterlies and prevailing easterlies from central Africa. On a large scale, the Sahara Heat Low, extending anomalously far to the northeast towards Libya during large parts of October 2019, appears to have facilitated the recurrence of such transient vortices by establishing an environmental setting usually found during peak monsoon in August. Eventually, a tropical–extratropical interaction coincided with the wettest period of the month over the Cameroon Highlands. Dry and initially cool air masses were advected equatorward from the Mediterranean towards the study region, contributing to the last strong episode of MFC linked with the landslide event. Subsequently, tropical–extratropical interactions were also involved in the termination of the rainy season. This study highlights not only the importance of the extratropics for rainfall variability in the African inner tropics, but also points to the hitherto understudied role of recurring vortex couplets over western tropical Africa and the Gulf of Guinea for multiday wet spells.

## KEYWORDS

Cameroon, cold surge, Gulf of Guinea atmospheric vortices, multiday wet spells, Sahara Heat Low, tropical–extratropical interactions

# 1 | INTRODUCTION

Landslides are common in the mountains along the Cameroon Volcanic Line (Zangmene et al., 2023). A landslide is the mass movement of rock, debris, earth, or mud down a slope. While most landslides are due to gravity, they can also be generated by precipitation, earthquakes, volcanic eruptions, groundwater pressure, erosion, and destabilization of slopes resulting from deforestation, agriculture and construction (Marc et al., 2022). Debris and mudflows are among the fast-moving landslides that are particularly dangerous because of their speed and volume. Landslides are distinguished from other terrain movements by clear boundaries and a significantly higher speed (Zangmene et al., 2023). Therefore, it is important to identify areas vulnerable to landslides and establish an early-warning system. On 29 October 2019, around 50 people died in a landslide in the regional capital city of Bafoussam (Figure 1), located in the Cameroon Highlands (Aretouyap et al., 2021). The National Meteorology Service of Cameroon reported that excessive heavy rains in the area contributed to this catastrophe. The extreme rainfall on 29 October was the culmination of a wet episode lasting one week (since 22 October) affecting several cities of the Cameroon Highlands, including Bafoussam and Dschang. Moreover the whole of October 2019 was extremely wet, not only in this region, but in many regions of equatorial Africa as documented in Nicholson et al. (2022). Given the susceptibility of the region to rain-induced landslides, extreme daily and multiday rainfall events need to be better understood and finally forecasted. An overall goal of the present study is to disentangle the meteorological drivers of the submonthly wet spells in the Cameroon Highland region.

Cameroon's climate is characterized by a varied spatial and temporal rainfall pattern and well-defined seasonality, with annual accumulated rainfall decreasing from south to north and from the coast to the mainland. The forest region of southern Cameroon has a bimodal rainy season, while elsewhere in the country rainfall is unimodal with August being generally the wettest month. The African rainbelt usually arrives in southern Cameroon in March and reaches its most northerly position in August. It then begins to withdraw equatorward around mid-September and early October. At the local scale, topography contributes significantly to rainfall modulation. On a large scale, the location and strength of the Sahara Heat Low (SHL) as well as changes in the Walker circulation, are among the drivers of rainfall variability in Cameroon (Cook & Vizy, 2015; Dunning et al., 2018). Seasonal rainfall is also modulated by the Indian Ocean Dipole (IOD, Moihamette et al., 2024), the South Atlantic Ocean Dipole (SAOD, Nana et al., 2023) and their interactions

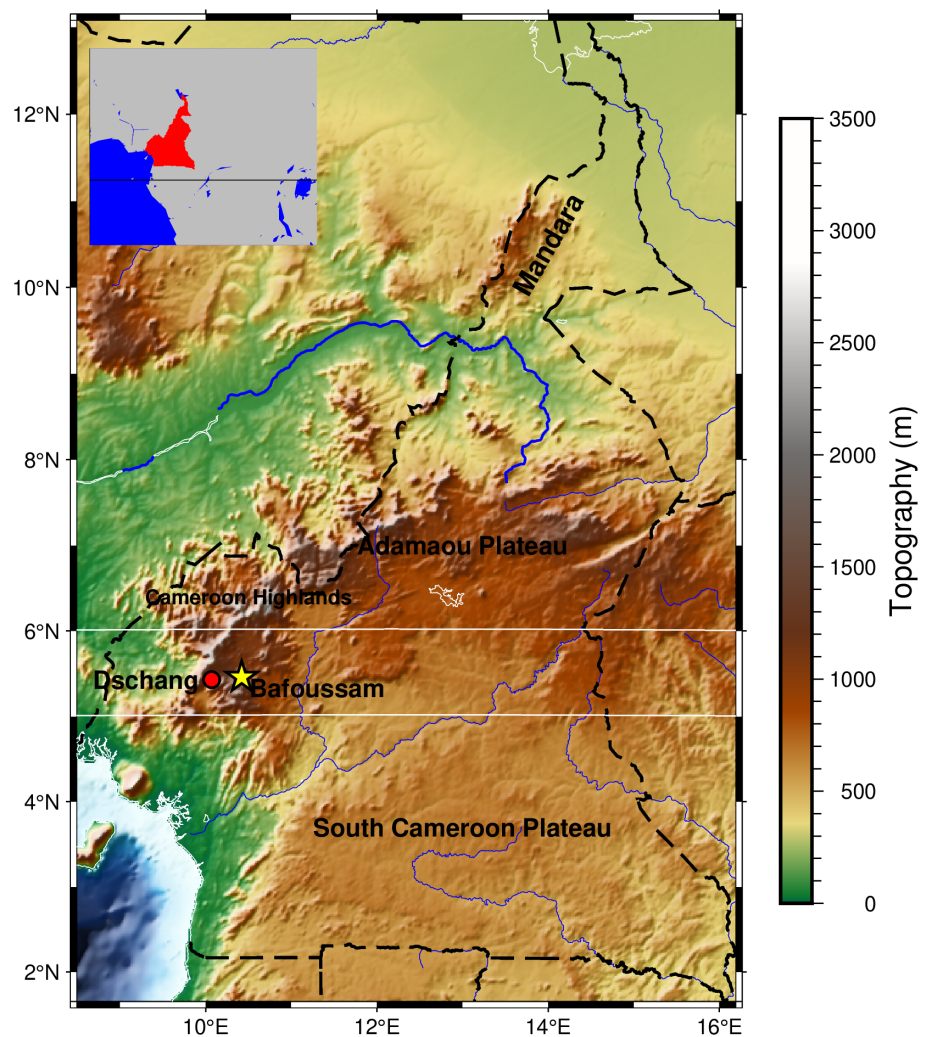
with the SHL as well as with the Intertropical Discontinuity (ITD). Tropical waves are also important drivers of rainfall in equatorial Africa. These waves contribute significantly to the synoptic to intraseasonal variability of tropical convection (Schlueter et al., 2019). The passage of convectively coupled Kelvin waves (Ayesiga et al., 2021) especially impacts synoptic-scale rainfall patterns over Central Africa. On the intraseasonal time scale, the Madden-Julian Oscillation (MJO) impacts rainfall in Cameroon (Wamba et al., 2023).

In order to understand climatological as well as seasonal to intraseasonal variations of rainfall in the rainbelt over equatorial Africa, previous studies have concentrated on the atmospheric water budget, that is, looking at moisture source, transport and convergence. Pokam et al. (2011), for example, show that seasonal variations of the spatial gradient of precipitation are modulated by moisture flux direction and strength. Also, annual cycles of precipitation are controlled by variations of moisture transport and evapotranspiration. The study of Tamoffo et al. (2022) has been devoted to analyzing the roles played by moisture supply for precipitation over equatorial Africa. These previous works have pointed out that the water vapour over Cameroon is advected from the Atlantic Ocean driven by the low-level southwesterly monsoon flow, and from the Indian Ocean driven by the midlevel African Easterly Jet (AEJ). Another important source of moisture in the region is the Congo Basin forest zone. The moisture from evapotranspiration within the forest canopy contributes significantly to the provision of water vapour in the region (Crowhurst et al., 2020). Yet, with the exception of studies on Kelvin waves (e.g. Zebaze et al., 2017), studies looking at submonthly drivers of moisture budget variations and multiday wet spells in equatorial Africa are lacking.

October and November 2019 were characterized by unusually high rainfall in tropical Africa (Kenfack et al., 2024). To explain the mechanisms that led to this wetness, Nicholson et al. (2022) analyzed potential drivers for this rainfall excess at the monthly scale. The IOD had its most positive value since the 1950s and was identified as a major driver of the wetness in eastern equatorial Africa. An unusually persistent Atlantic Niño event was suggested to have contributed to the wetness along the Guinea and western equatorial Africa coast south of the equator (Vallès-Casanova et al., 2020). In terms of the equatorial Walker circulations, Nicholson et al. (2022) show anomalous rising branches over parts of equatorial Africa that were related to the IOD and Atlantic Niño anomalies. Furthermore, the SHL was located anomalously far east and north in October 2019. Correspondingly, a stronger than usual AEJ and the ITD were also in anomalously northern positions. In western North Africa east of the



**FIGURE 1** Topography (m) of the study region from Global Earth Relief 01 m (Tozer et al., 2019). The two weather stations Dschang (red circle) and Bafoussam (yellow star) are indicated. The two horizontal white lines delineate the longitudinal transect for which the Hovmöller plot will be represented in Figure 4. The landslide occurred near Bafoussam on 29 October 2019. [Colour figure can be viewed at [wileyonlinelibrary.com](https://onlinelibrary.wiley.com/doi/10.1002/qj.70066)]



Greenwich meridian, African Easterly Wave (AEW) activity was anomalously strong and may have contributed to the wetness in this region. Overall, the whole West African monsoon system was displaced north of its climatological position in the monthly mean, thus allowing strong southwesterly moisture fluxes from the Atlantic Ocean to enter the study region. Finally, Nicholson et al. (2022) showed evidence of less prominent tropical wave activity over equatorial Africa during October 2019 compared to November 2019.

While the study of Nicholson et al. (2022) yields evidence for the extreme wetness of October and November 2019, which was accompanied by a record number of weather disasters in Africa, it lacks the regional and sub-monthly perspective and a more in-depth study of drivers of multiday wet spells. It shall be mentioned in this context that previous studies have dealt with extreme, daily rainfall based on isolated cases (e.g., Igri et al., 2018; Maranan et al., 2019; Mouassom & Tamoffo, 2024; Moudi et al., 2023; Osei et al., 2022; Osei et al., 2023) often related to westward-propagating mesoscale convective systems.

The present study aims for a more in-depth analysis of drivers of the multiday wet spells in October 2019 that ultimately led to the devastating landslide in Bafoussam. It will adopt examinations at a local to continental scale and look at tropical and extratropical drivers. It will be shown that the latter were a major factor in explaining both the wettest period at the end of the month, but also the end of the wetness by contributing to the termination of the 2019 rainy season. The remainder of the paper is organized as follows: Section 2 describes the datasets and methodology, while the results are presented in Section 3. Discussions and conclusions are given in Section 4.

## 2 | STUDY REGION, DATA AND METHODS

### 2.1 | Study region

The present study mainly focuses on the region of the October 2019 landslide event, that is, the western part

of the Cameroon highlands, around the cities of Bafoussam and Dschang (Figure 1), both of which are densely populated areas with more than 450,000 (World Population Review, 2024) and 70,000 inhabitants, respectively. The uneven elevation of the region is about 1400 m above sea level, covered with vegetation typical for the tropical savannah climate. The slopes of the hills in the Bafoussam area are steep in some places, facilitating erosion and potential landslides due to degradation of vegetation cover (Aretouyap et al., 2021). Bafoussam (Dschang) receives an annual mean precipitation of about 2200 mm (2030 mm) during approximately 110 (190) rainy days (Kengni et al., 2019; Molua, 2006). Both stations have a unimodal precipitation regime with a start of the rainy season in mid-March and a termination in mid-November. The rains are associated with the low-level moist southwesterly monsoon flow from the Atlantic Ocean. The wettest months are July, August and September, with more than 200 mm of monthly accumulated rainfall (Molua, 2006).

## 2.2 | Rainfall datasets

This study leverages daily (0600–0600 UTC) rainfall data from the weather stations in Bafoussam (5°29' N, 10°26' E, 1401 m) and Dschang (5°26' N, 10°02' E, 1330 m). The rainfall data for October 2019 were collected from the Department of National Meteorology of Cameroon. The historical rainfall data for the stations, ranging from 1943 to 1986 for Bafoussam and from 1948 to 1980 for Dschang, were extracted from the Karlsruhe African Surface Station Database (KASS-D, Vogel et al., 2018). These historical data were used to calculate the 95th and 99th percentile levels of rainfall to assess the extremeness of precipitation periods during October 2019. Daily rainfall data from the 1990s to recent from both stations were not available to us.

In addition to in-situ observation data, this study also uses satellite-based precipitation estimates to provide a spatially extended regional perspective of the October 2019 rainfall. Here, the latest version 7 of the Integrated Multi-satellite Retrievals for GPM (IMERG hereafter, V07 final run; Huffman et al., 2023) dataset is utilized, which is a globally gridded precipitation product that integrates data from a variety of sources within the Global Precipitation Measurement (GPM) mission constellation satellite network (Maranan et al., 2020; Tan et al., 2016). The GPM satellite observation network, centring around the GPM Core Observatory satellite and hosting a dual-frequency precipitation radar (DPR) as well as a 13-channel partner passive microwave (PMW) imager (GMI), is augmented by multiple PMW instruments within the GPM constellation and infrared (IR) information from geostationary satellites

(Maranan et al., 2020; NASA, 2023). Rainfall estimates from IMERG are processed on a 0.1° grid at 30-minute intervals (Bulovic et al., 2020). Notable changes between versions 6B and 7 include: a bug fix of a spatial offset in gridding precipitation information; an improved intercalibration of PMW estimates; and changes in the morphing scheme by using the SHARPEN technique (Tan et al., 2021). In the present study, IMERG daily rainfall data for the October months 2000–2019 were accumulated for the 0000–0000 UTC period.

Finally, as a proxy for tropical deep convection and associated rainfall, the daily (2.5° × 2.5°) interpolated National Oceanic and Atmospheric Administration (NOAA) outgoing longwave radiation (OLR) dataset (Liebmann & Smith, 1996) is used for the identification of convectively coupled equatorial waves (CCEWs). This is achieved through a spectral wave filtering method outlined in Section 2.4.

## 2.3 | Reanalysis data

The fifth generation of the European Centre for Medium-range Weather Forecasts (ECMWF) reanalysis series, ERA5 (Hersbach et al., 2020), is used in this study to investigate the regional and large-scale dynamics leading up to the rainfall episodes in October 2019. The Integrated Forecasting System (IFS, cycle 41r2) model produces three-dimensional meteorological fields from a hybrid, incremental, four-dimensional variational data assimilation scheme. ERA5 data are publicly available from the year 1940 onwards and are constantly extended forward in near real-time. They are based on two forecasts made each day at 0600 and 1800 UTC. ERA5 is provided on an hourly basis and on a 0.28125° × 0.28125° spatial grid. For practical reasons, the data were retrieved at a grid spacing of 0.25° × 0.25°. We averaged or, in the case of precipitation, aggregated the hourly ERA5 data from 0000 to 00000 UTC, both for October 2019 and for the reference period October 2000–2018, the latter of which overlaps with the reference period of the IMERG data. Surface and upper-air data from the ERA5 reanalysis were employed, including the three-dimensional wind components ( $u$ ,  $v$ ,  $\omega$ ), 2-m temperature ( $t_2m$ ), the zonal and meridional components of vertically integrated water vapour transport and its divergence (VIMD), mean sea level pressure (MSLP), the total precipitable water (TPW), geopotential height ( $z$ ) and precipitation. The precipitation estimates from ERA5 are from the short-range background forecasts used to provide the standard ERA5 precipitation product. To obtain 24-hour precipitation estimates, the short-range background forecasts use accumulations from the first 12 hours of forecasts from 0600 and 1800 UTC.

## 2.4 | Methods

This study defines a rainy day as having a valid rainfall record greater than zero. In the calculation of rainfall percentiles for both station and IMERG data, only rainy days were considered. The percentiles for the negative values of VIMD, indicating convergence, were calculated separately from the positive values of VIMD, which represent divergence. Thus, negative percentiles are possible for which large values indicate strong convergence. For the sake of convenience, we will refer to negative VIMD as moisture flux convergence (MFC) hereafter. The data recorded in October 2019 were used to determine the percentiles to which they correspond relative to the reference period 2000–2018. As mentioned above, this period is chosen to match the IMERG rainfall sample. For a given period and for each day, daily anomalies are obtained by subtracting the average of the daily climatological data for October from  $t$  corresponding daily value in October 2019.

The spatial distribution of the anomaly of precipitation during wet spells is analyzed. To allow for a meaningful comparison across the study area, anomaly values are divided by the maximum absolute anomaly at each grid point. The normalization scheme is realized based on Equation (1), where  $X_{2019}$  (for day  $i$ ) and  $X_{Clim}$  (for day  $i$ ) are, respectively, rainfall recorded in 2019 and climatology at each grid point. We added infinitesimal  $\epsilon$  to the denominator to prevent division by zero.

$$100 \cdot \frac{X_{2019} - X_{Clim}}{\max(|X_{2019} - X_{Clim}|) + \epsilon} \quad (1)$$

Finally, a spectral tropical wave analysis was conducted to investigate potential links between the October 2019 rainfall and the existence of CCEWs. Wave signals are detected using fast Fourier transformation filtering technique in the wavenumber–frequency domain (Wheeler & Kiladis, 1999). The wavenumber–frequency windows for each wave mode are equal to those in Schlueter et al. (2019). The investigated tropical waves include Madden–Julian oscillation (MJO), Kelvin waves, tropical disturbances (TD), mixed Rossby–gravity waves (MRG), equatorial Rossby waves (ER), and eastward-propagating inertio–gravity waves (EIG).

## 3 | RESULTS

While Nicholson et al. (2022) investigated the causes of the intense October and November rainfall in 2019 in a monthly and pan-equatorial African context, this study focuses on the evolution of precipitation in the western Cameroon highlands on a submonthly to daily

basis. In the following, the October 2019 rainfall evolution around the stations of Bafoussam and Dschang is presented first before important aspects of regional to large-scale (thermo-)dynamics leading up to these heavy rains are highlighted.

### 3.1 | Rainfall characteristics during October 2019

In October 2019, the stations Bafoussam and Dschang measured a total accumulated rainfall amount of 526.4 mm and 810.3 mm, respectively. A time series of daily accumulated precipitation at the two stations and horizontal maps of IMERG-based rainfall are presented in Figure 2. At both Bafoussam and Dschang, a high number of wet days were registered: 18 days for Bafoussam and 21 for Dschang. Taking the 99th percentile of daily October rainfall, that is, 54.15 mm (51.52 mm) at Bafoussam (Dschang, solid lines in Figure 2a) as a reference, multiple rainfall days at both stations were extreme. Moreover, it is evident that extreme rainfall occurred on successive days on several occasions in Dschang. This is even more pronounced at the 95th percentile, that is, 35 mm (37.5 mm) at Bafoussam (Dschang, dashed lines in Figure 2a). Overall, even though large differences in daily rainfall are notable despite the proximity of Bafoussam and Dschang, three marked common multiday wet spells can be subjectively identified (grey-shaded areas), which contribute to the majority of the October 2019 rainfall. The first wet spell begins on 1 October and lasts until 6 October. The second wet spell covers the period from 8 October to 14 October. Lastly, the third wet spell ranges between 22 October and 30 October. As seen later, the end of the third wet spell also marks an abrupt termination of a region-wide wetness and the rainy season of 2019. The extreme one-day rainfall event recorded on 19 October at both stations was not included in any wet spell, as it occurred largely isolated.

To obtain an overview of how monthly rainfall at Bafoussam and Dschang is placed in a regional context, Figure 2b shows the difference between October 2019 and a long-term October mean (2000–2018) as seen by IMERG. Over the Cameroon Highlands and the Adamaoua Plateau, there is an excess in monthly rainfall, reaching up to 250 mm. This positive anomaly is clearly aligned with the shape of the mountain range and indicates the influence of orographic rainfall enhancement. However, it is accompanied by an extensive area of below-average monthly rainfall in the south of Cameroon, where the dry anomaly is most pronounced in the coastal region with a monthly rainfall deficit of over 250 mm. A marked positive rainfall anomaly appears to the east of the dry anomaly towards the border with the Central



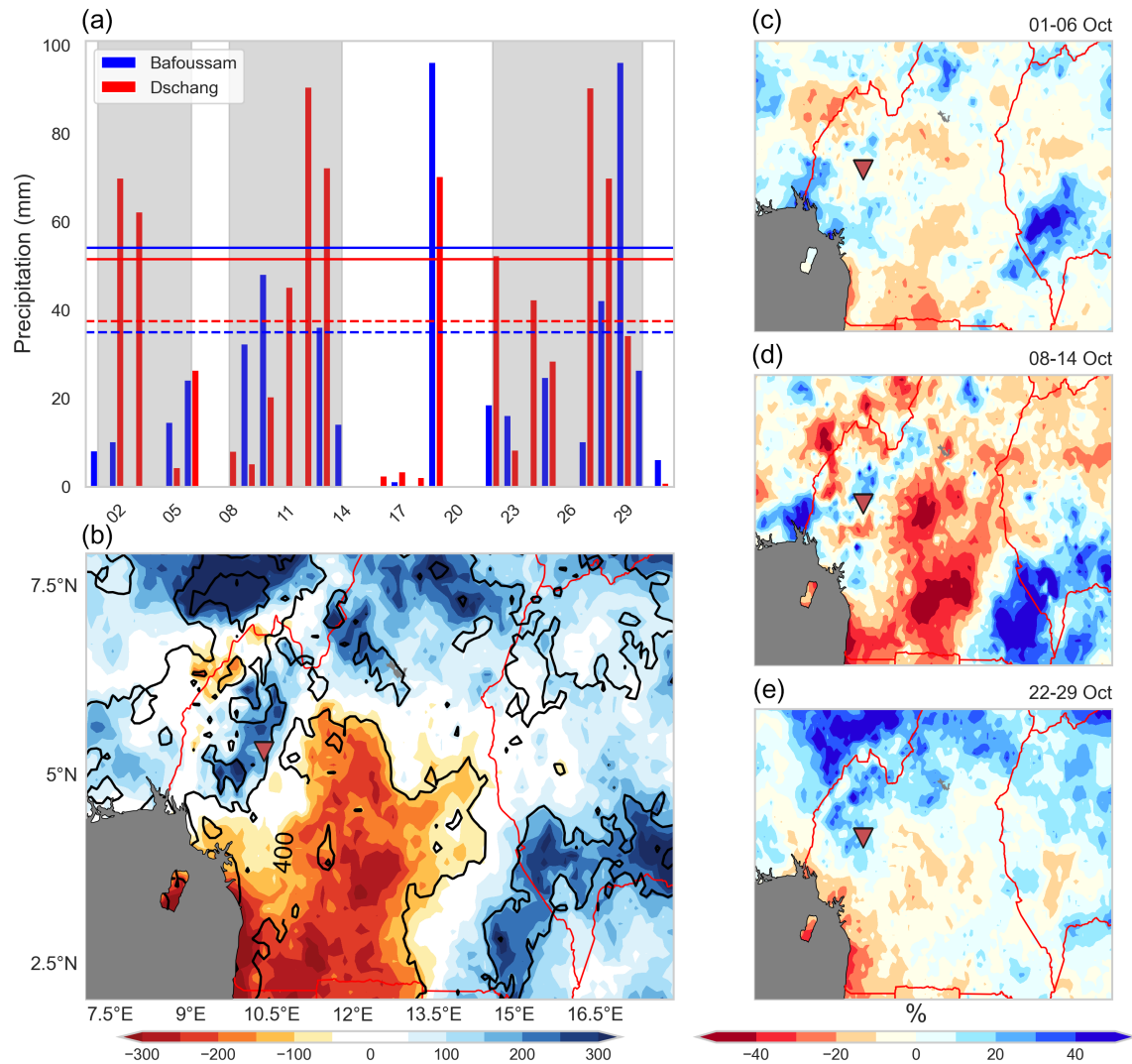


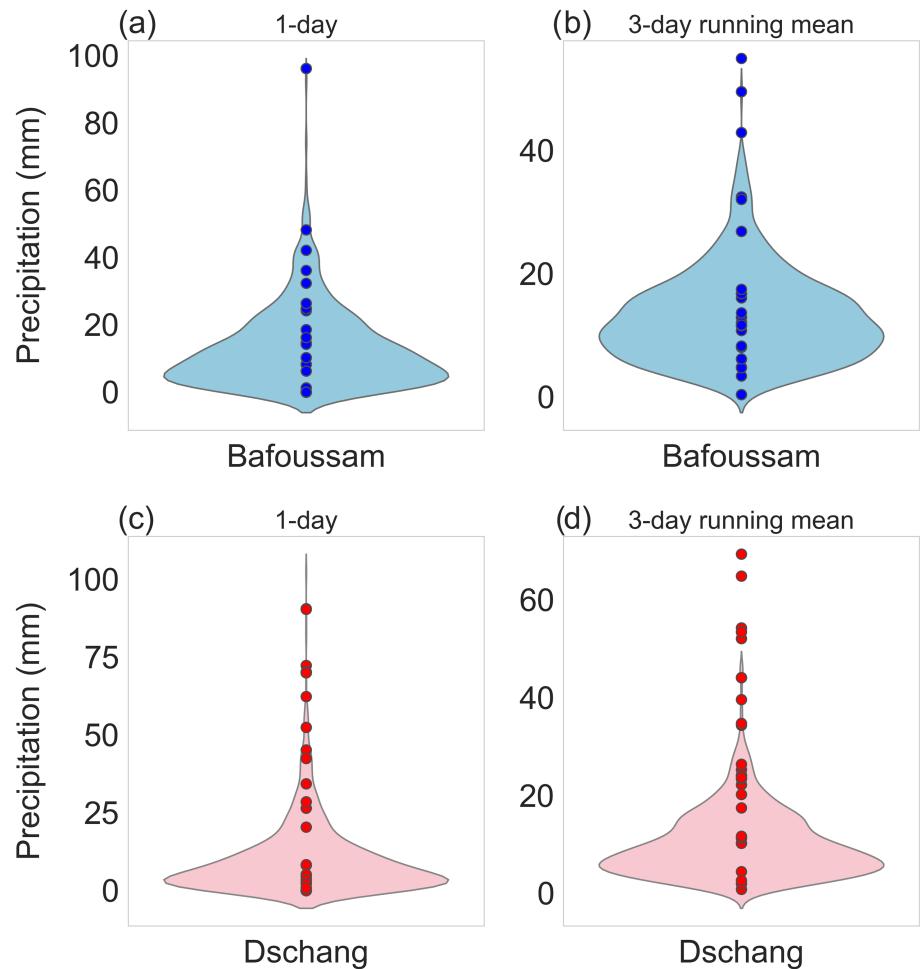
**FIGURE 2** Breakdown of the October 2019 rainfall (mm) in the study region (a) Time series of daily rainfall at Bafoussam and Dschang during October 2019. The dashed (continuous) horizontal lines indicate the 95th (99th) percentile of daily October 2019 rainfall with respect to the 2000–2018 reference period. (b) Rainfall anomalies in October 2019 vs the October 2000–2018 mean with black contours indicating accumulated total rainfall. (c–e) Multiday precipitation anomalies in percent during October 2019 relative to October 2000–2018 from IMERG. The location of Bafoussam is marked with a red triangle. Grey shading in (a) highlights the three wet spells during October 2019. [Colour figure can be viewed at [wileyonlinelibrary.com](https://onlinelibrary.wiley.com/doi/10.1002/qj.70066)]

African Republic at the fringes of the Congo Basin. Despite a different rainfall dataset and reference period for the long-term mean, this anomaly pattern is largely in line with findings in Nicholson et al. (2022). In Figure 2c–e, the individual rainfall anomalies during the three wet spells, represented as percentage deviations from the long-term mean, are evaluated. Here, we normalized the anomaly at each grid point by the maximum absolute value of the daily anomaly at the considered grid point (Equation 1). In general, the distinct anomaly structures in Figure 2b stem from different wet spells during October 2019, for example, the extensive dry–wet anomaly dipole between western equatorial Africa and the Congo basin

imprinted by the second wet spell (Figure 2d), and the wet anomaly in the northern part during the third wet spell (Figure 2e), the potential causes of which are investigated in Section 3.4. The commonality among all wet spells is the anomalously wet mountain range (Figure 1: Cameroun Highlands, Adamaoua Plateau), indicating the role of orography for enhanced rainfall that may have led to the devastating landslides at the end of October 2019.

Violin plots were created to put the daily and multiday rainfall accumulations at both stations in October 2019 into the climatological context. Figure 3 presents a comparison between the October 2019 daily (Figure 3a,c)

**FIGURE 3** Violin plots illustrating the probability distributions of October daily and three-daily precipitation for the KASS-D historical periods. Dots are for October 2019. Panels (a,b) and (c,d) show the daily and three-daily distribution for Bafoussam and Dschang, respectively. For the three-daily statistics a three-day running mean has been employed. [Colour figure can be viewed at [wileyonlinelibrary.com](https://onlinelibrary.wiley.com)]



and three-daily (Figure 3b,d) rainfall totals (dots) and the long-term distribution (violin plots). As elucidated in Figure 2a already, it is evident that several daily rainfall totals in October 2019 are located in the high-percentile range which is particularly true for Dschang (Figure 3c). However, none of the daily values at either Bafoussam and Dschang represent or exceed the maximum value in the KASS-D sample. In contrast, it is the intensity of three-day aggregated rainfall that sets 2019 apart from other historical years. Considering three-day running mean values in Figure 3b,d, the maximum values of the historical sample are exceeded on several occasions at both stations. These intense three-day precipitation values characterize the three major wet spells of October 2019 (cf. Figure 2a). We also tested the two-day, five-day and seven-day moving averages and the maximum cumulated values in October 2019 are always higher than the maxima of historical data. The three-day average smoothed out the data less and kept the basic trend.

To further extend the perspective of the three-day running rainfall and its intensity, Figure 4a shows a Hovmöller diagram of the three-day IMERG-based percentile values for October 2019 in comparison to the reference 2000–2018 at every available longitude between 5° E and 25° E. For

this purpose, rainfall was averaged in a meridional band from 5° N to 6° N (see Figure 1). At the longitude of Bafoussam and Dschang at around 10° E (black vertical line), several high-percentile rainy episodes are also registered by IMERG and largely fall within the three defined wet spells (grey-shaded areas). Signals at the end of the third wet spell appear particularly strong and reach percentile values close to 100. Furthermore, it is noteworthy that within the wet-spell periods defined based on station data at Bafoussam and Dschang, central equatorial Africa east of 15° E towards the Congo Basin also experienced extensive and intense wet episodes. Another rainy period is registered by IMERG around 19 October, which is reflected by only one isolated but intense one-day rainfall event in the station data (see Figure 2a). We note that while it shares similar characteristics regarding its zonal extent, the focus of upcoming examinations will remain on the defined station-based wet spells. Finally, a widespread abrupt end of (intense) rainfall activity is visible from the beginning of November onwards and suggests a complete change in the dynamical regime towards early dry season conditions.

Figure 4b shows the percentile values of the three-day averaged VIMD where high positive (negative) values indicate increased moisture flux divergence (MFC).



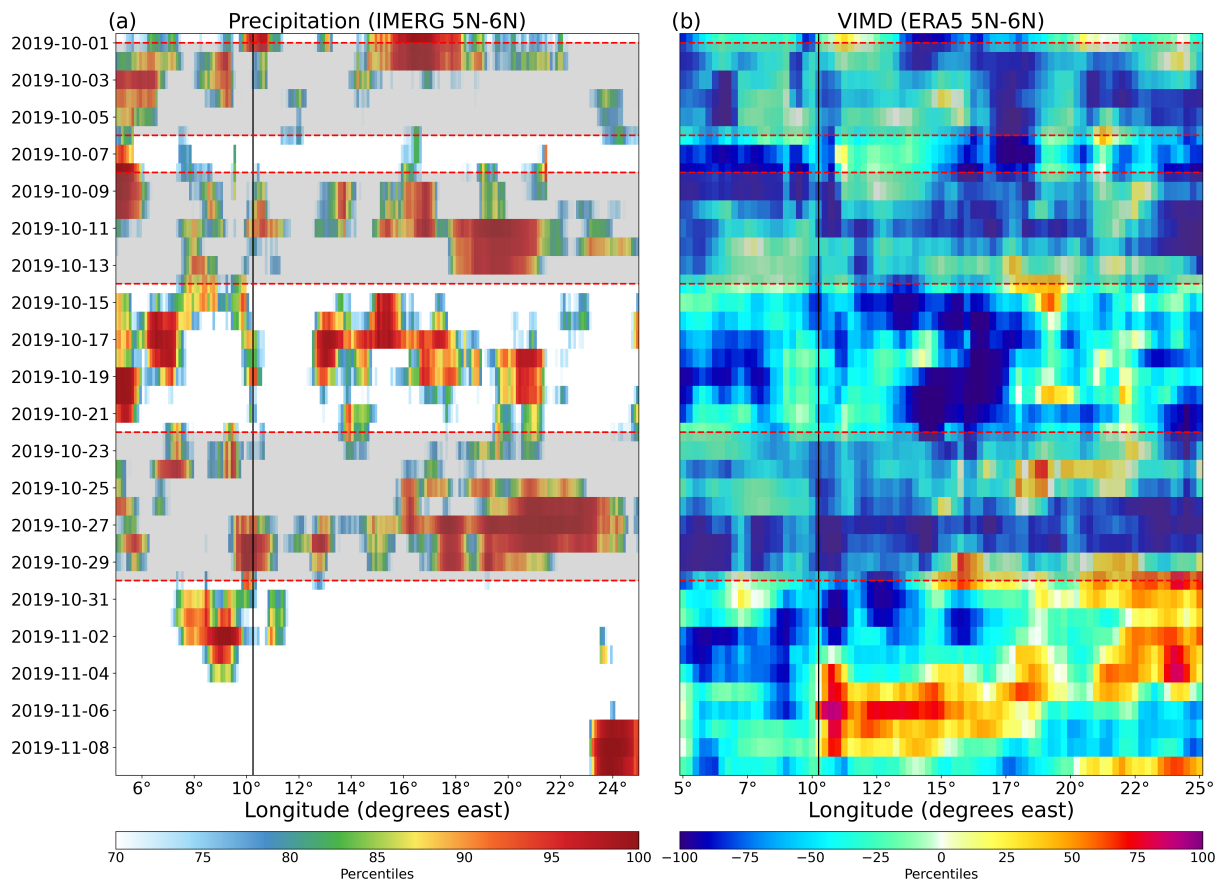


**FIGURE 4** Hovmöller diagrams of (a) the percentiles from three-day running means of IMERG rainfall (mm), and (b) the vertically integrated moisture divergence (VIMD,  $\text{kg}\cdot\text{m}^{-2}\cdot\text{s}^{-1}$ ) during October 2019 averaged between 5° N and 6° N. Negative VIMD percentile values represent convergence. The vertical black line indicates the longitude of Bafoussam and Dschang. Grey shadings in panels (a) and (b) highlight wet spells during October 2019. [Colour figure can be viewed at [wileyonlinelibrary.com](https://onlinelibrary.wiley.com/doi/10.1002/qj.20066)]

A strong relationship between intense rainfall and high-percentile MFC becomes evident. Particularly the third wet spell is marked by pronounced MFC spanning the entire zonal domain, resulting in the aforementioned spatially extensive rainfall. Eventually, the termination of the wet month of October 2019 in the study area coincides with the occurrence of a zonally extensive band of intense moisture divergence over and east of the study region.

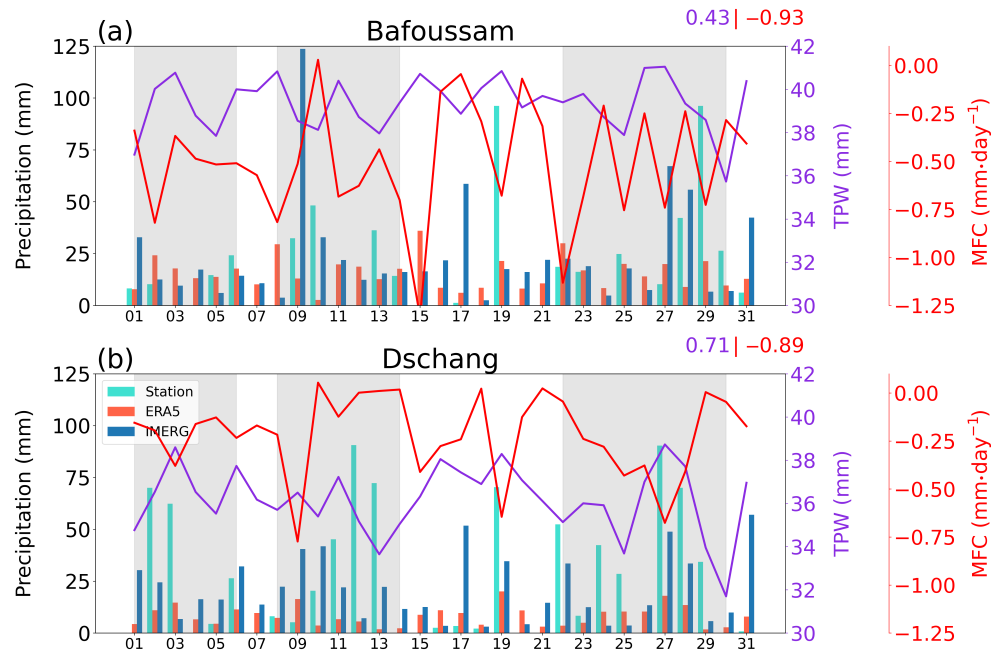
Our results indicate that MFC over the Cameroon Highlands was an important factor in the development of convection and extreme rainfall. The question now is what mechanisms are in place that facilitate this level of MFC?

### 3.2 | Circulation and moisture

In the previous section, we identified strong MFC as one of the facilitators for intense rainfall in the study domain. More insight into this relationship is given in Figure 5, which shows daily time series during October 2019 for the vertically integrated MFC (red curve), TPW (purple curve), and rainfall from stations, IMERG, and ERA5 (green,

blue, red bars, respectively) at Bafoussam (Figure 5a) and Dschang (Figure 5b). It must first be noted that there is a discrepancy in magnitude and timing on a point-to-pixel observational level between stations, IMERG and the model-driven ERA5 rainfall. This highlights the highly variable and difficult quantification of precipitation in space and time, and in particular in the tropical and mountainous setting around Bafoussam and Dschang. Nonetheless, ERA5 exhibits rainfall every day. This is in agreement with IMERG, reflecting the overall wet character of October 2019 over the Cameroon Highlands. Comparing the evolution of ERA5 rainfall with that of MFC, a high anti-correlation of  $-0.93$  ( $-0.89$ ) at Bafoussam (Dschang) is found. The strongest daily ERA5 rainfall is almost always associated with pronounced MFC. At the same time, ERA5 rainfall is moderately correlated with TPW with a value of  $0.43$  ( $0.71$ ) at Bafoussam (Dschang). Thus, the interplay between these three components, where marked MFC coincides with peaks in TPW and eventually rainfall, gives rise to the question of how enhanced MFC in the context of multiday wet spells is created in this region.

**FIGURE 5** October 2019 daily time series of rainfall shown as bars for rain gauges (turquoise), ERA5 (orange), IMERG (blue) together with lines of total precipitable water (purple) and of moisture flux convergence (red) in Bafoussam (a) and in Dschang (b). The Pearson correlation coefficient between ERA5 rainfall and total precipitable water (moisture flux convergence) is shown in purple (red) at the top-right. Grey shading highlights wet spells during October 2019. [Colour figure can be viewed at [wileyonlinelibrary.com](https://onlinelibrary.wiley.com)]



For all three wet spells, Figure 6 depicts the absolute fields (respective upper rows) of vertically integrated moisture flux (vectors) and VIMD (shaded) at selected days in October 2019, and their anomaly fields (respective lower rows) based on the 2000–2018 October climatology. The columns represent three approximate phases of each wet spell, namely (pre-)onset (left column), peak moisture flux (middle column), and ending stage (right column). Across the three wet spells, the setting during the (pre-)onset phase in the absolute fields (Figure 6a,g,m) includes a cyclonic circulation (marked with a blue ‘V’ throughout the panels) east of the Bafoussam and Dschang stations over east Cameroon and/or the northern Congo Basin. In fact, auxiliary analyses of the October 2019 moisture flux fields have shown regular generation of cyclonic features over the northern fringes of the Congo Basin and the eastern part of the Cameroon Highlands (not shown). While the identification of their sources is beyond the scope of this study, cyclonic structures can coincide with the occurrence of enhanced convective activity, as seen, for instance, in the region of convection-driven MFC for the third wet spell (Figure 6m). As also seen in the anomaly fields (Figure 6d,j,p), the (pre-)onset phase is marked by northerly-to-northeasterly moisture fluxes into the study region. Towards the second phase (middle column), these cyclonic features, which generally vary in size, intensity, and position, move westward over the Guinea coast and intensify as they pass the study region. As a consequence, enhanced oceanic southwesterlies in the form of extensive cross-equatorial moisture transport towards the Cameroon Highland prevail (Lin et al., 2017; Rodwell & Hoskins, 1995). Studying them indicated that maintaining an irreversible cross-equatorial flow

depends on the alteration of potential vorticity within the low-level monsoon winds. Furthermore, the second wet spell is marked by a second vortex located further south over the equatorial African coast (Figure 6h, denoted by ‘V\*’) which, together with a distinct northern position of the cyclonic vortex at around 10° N, facilitates anomalous southwesterly moisture transport into the Sahel (Figure 6k). At the same time, this southern vortex likely caused the distinct dry anomaly over western equatorial Africa by diverting moisture away from this region (cf. Figure 2d). While the development of these southern vortices has not been investigated in detail in this study, they were prominent features along the eastern equatorial Atlantic during October 2019 (not shown) which, as also seen in Knippertz et al. (2017), can generally be part of westward-moving vortex couplets along the Guinea coast region. Overall, the second phase features strong MFC, which is widespread in some areas of the study region. While MFC is likely generated by orographic lifting already, a further enhancement is likely linked to the convergence of the southwesterlies with the trailing easterlies from central Africa which becomes most apparent for the third wet spell (Figure 6n). Eventually, the ending phase (right column) of the wet spells is largely characterised by the westward departure of the cyclonic vortex, the breakdown of the southwesterlies, and the transition to an easterly flow regime, thereby reducing and eventually terminating onshore moisture transport in the study area. In summary, the evolution of all wet spells during October 2019 was dominated by transient, westward-moving cyclonic vortices which dictated the onset and magnitude of moisture transport and MFC in the study region.

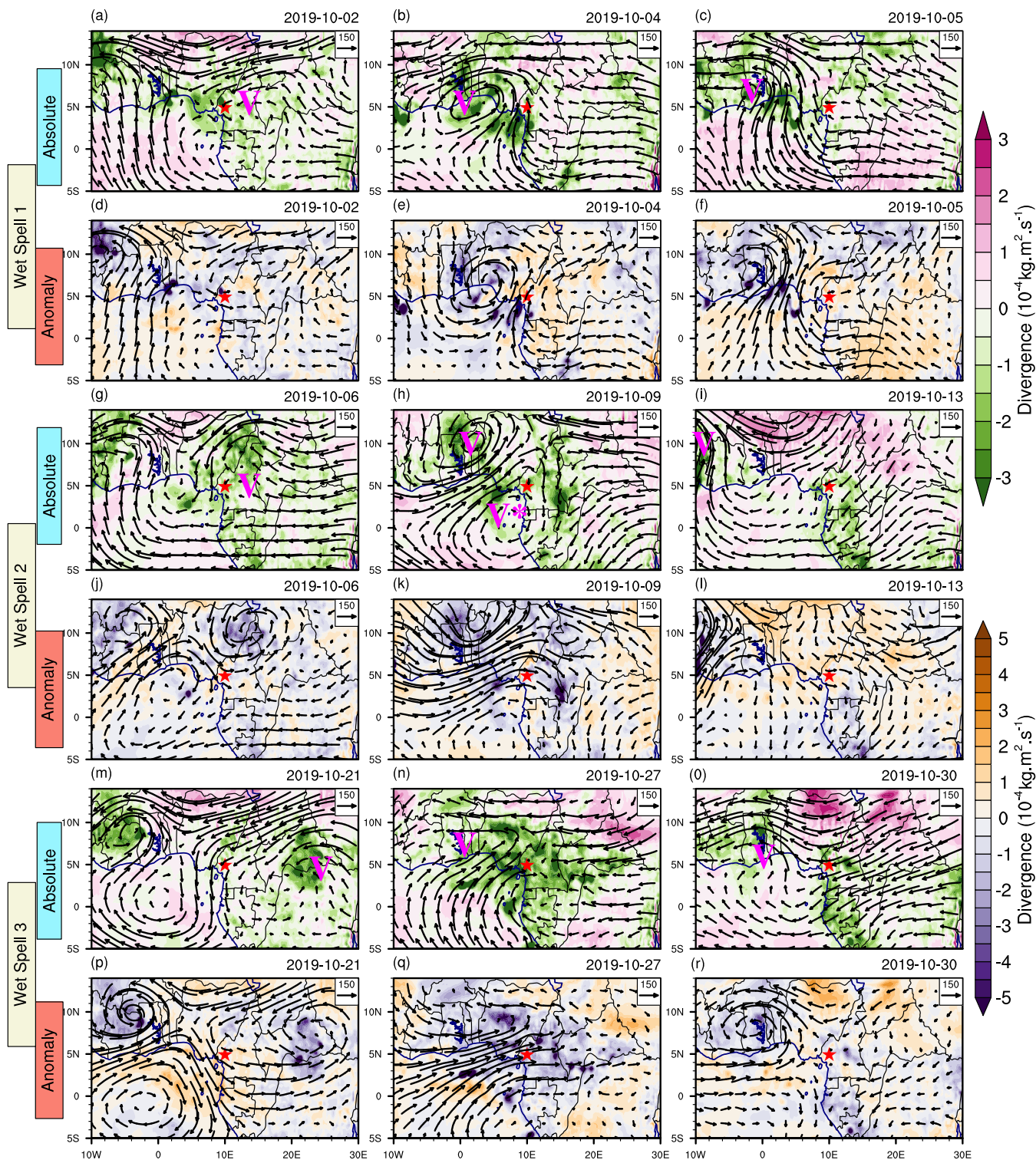


**FIGURE 6** Absolute and anomaly fields of the daily mean value of the vertical integral of water vapour flux (vectors:  $\text{kg}\cdot\text{m}^{-1}\cdot\text{s}^{-1}$ ) and the vertically integrated moisture divergence (shaded:  $\text{kg}\cdot\text{m}^{-2}\cdot\text{s}^{-1}$ ) during the three wet spells identified in October 2019. The left, middle, and right column show the (pre-)onset, peak moisture flux, and ending phase, respectively, of each wet spell. The days representing the phases are indicated on the top right of each panel. Negative and positive values indicate moisture convergence and divergence, respectively. The red star indicates the position of Bafoussam. The 'V' marker denotes the location of the cyclonic vortex feature, the 'V\*' marker the secondary vortex during the second wet spell. [Colour figure can be viewed at [wileyonlinelibrary.com](https://onlinelibrary.wiley.com/doi/10.1002/qj.20066)]



### 3.3 | Seasonal to synoptic-scale drivers of rainfall

This section extends the perspective to the large scale and explores potential synoptic drivers for the prevalence of rainfall during the wet spells. Figure 7a–c show anomaly fields of MSLP (shaded) for three selected days. In general, the large-scale setting during the wet spells in October 2019 is dominated by a well-defined negative MSLP anomaly covering large parts of Libya and northern parts of Sudan and Niger, and thus, suggesting an anomalously northeastward shift of the SHL (termed ‘SHL anomaly’ hereafter for convenience). The SHL anomaly appears relatively consistent in location and magnitude between the first and second wet spell (Figure 7a,b), as also reflected in the monthly perspective taken in Nicholson et al. (2022). Accordingly, an extensive warm anomaly, as seen in the t2m anomaly field for the same days shown in Figure 7d–f (shaded), is found with differences of over +3°C in the core area of the SHL anomaly. However, signs of its weakening as well as an equatorward penetration of anomalously cold air masses from Egypt become apparent for the third wet spell (Figure 7c,f). In anticipation of further details examined in Section 3.4, this is linked to the end of the wet conditions in the study area (cf. Figure 4a).

Potential implications of this strongly disturbed MSLP field on the large-scale moisture field is further evaluated through anomalies of TPW (contours in Figure 7a–c) and vertically integrated moisture flux (vectors in Figure 7d–f). The 14°C isodrosotherm (thick blue contour in Figure 7a–c) is also included as a proxy for the position of the ITD and thus the northern boundary of the moist monsoon layer (Fink et al., 2017; Lafore, 2017). As previously outlined, the cyclonic–anticyclonic vortex pair induces strong southwesterly moisture fluxes towards the Cameroon Highlands from anomalously warm air masses over the ocean (see 2-m anomalies in Figure 7d–f). This leads to positive TPW anomalies not only over the main study region, but also anywhere south of the ITD with a maximum at roughly +14 mm (Figure 7a–c). The strong and stable SHL anomaly during the first and second wet spell allows for a deep inland penetration of moist air, leading to a northward bulge in the ITD (approximately 15° N) south of the core of the SHL anomaly (Figure 7a,b). While this is also seen for the third wet spell, the ITD has slightly retreated southward as one sign of a weakening SHL anomaly at that stage (Figure 7c). Thus, while it is suggested that westward-propagating cyclonic vortices are major factors for the build-up of favourable conditions for wet spells over the Cameroon Highlands, an anomalously northeastward-shifted SHL is capable of not only intensifying the inland moisture flux (cf. Dunning et al., 2018; Knippertz & Fink, 2008) but also of establishing a suitable

environment for such recurring cyclonic vortices, which would be more typical for peak monsoon conditions in August.

Figure 8 provides a submonthly perspective of the zonally oriented vertical cross-sections of the climatology (left column) and anomaly (left column) of the zonal vertical flow (streamlines) and the vertical motions (omega; shaded), averaged over the three defined wet spells in October 2019 within the 5° S–5° N latitude band. Here, the climatology was determined with respect to 2000–2018 for the respective wet spells. The longitude of the study area is indicated by a vertical red dashed line for reference. Climatologically, ascending motions (blue shading) are found over large parts of the equatorial region of the African continent (Figure 8a–c), likely signatures of convective activity over both the East African rift and the extensive Congo Basin. Furthermore, deep easterlies above 850 hPa prevail that extend from the continent to the open waters of the Gulf of Guinea where descending motions dominate. The anomalies in October 2019 during the three wet spells highlight a considerably disturbed flow where deep westerlies from the Gulf of Guinea converge with the easterlies from the continent at the longitude of the Bafoussam and Dschang stations (dashed vertical red lines; Figure 8d–f), in line with analyses made in Figure 6. As a result, enhanced anomalous upward motions are prevalent into upper-tropospheric levels. A remarkable aspect, apart from the large zonal extent within the 5° N–15° N longitude band, is the depth of these anomalous convergent motions which reaches up until roughly 400 hPa before the flow turns westward at upper levels. Overall, the intensity of anomalous upward motions appears to be strongest during the second and third wet spells (Figure 8e,f), during which the more intense rain was recorded as compared to the first wet spell.

Tropical waves are among the factors that are capable of modulating the synoptic to intraseasonal variability of precipitation over western equatorial Africa (e.g. Sinclair et al., 2015; Schlueter et al., 2019; Ayesiga et al., 2021; Alber et al., 2023) by altering, among other things, the ambient conditions of moisture. They are known to be related to extreme daily rainfall (Peyrillé et al., 2023) in the central Sahel. Whether the activity of tropical waves was a source of the October 2019 wetness is examined in Figure 9, which shows a Hovmöller plot of OLR anomalies calculated for October 2019 minus October 2000–2018 (shaded) and active waves (i.e., in their wet (dry) phases; solid (dashed) contours). Again, the longitude of the Bafoussam and Dschang stations is indicated by a red dashed line. Convective activity over the study area, characterized by negative values of OLR anomalies (purple colour), prevails during large periods in October 2019, highlighting again the pronounced wetness in that month. However,

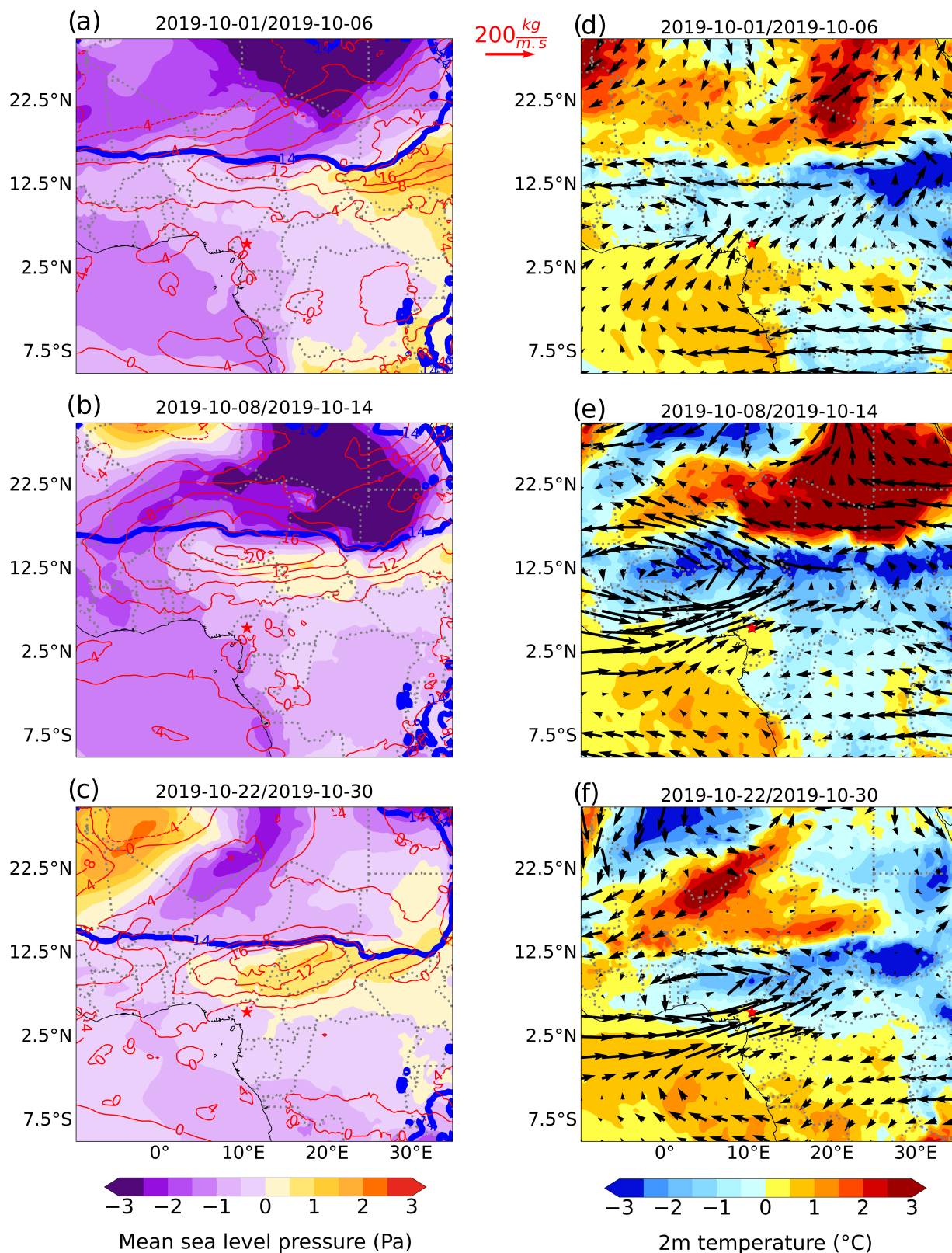


**FIGURE 7** Left column (a,b,c) shows anomalies of mean sea level pressure (shaded, in Pa) during the three October 2019 wet spells relative to 2000–2018. The red contours show anomalies of the total column vertically-integrated water vapour during October 2019 relative to 2000–2018. The blue contour denotes the 14°C dew-point temperature at 2 m during October 2019 as a proxy for ITD. The right column (d,e,f) shows anomalies of daily t2m (shaded, in °C) during October 2019 relative to 2000–2018. Arrows indicate the anomaly of the vertical integral of water vapour flux ( $\text{kg}\cdot\text{m}^{-1}\cdot\text{s}^{-1}$ ). The days on which each wet spell was detected are indicated in each panel heading. The red star indicates the position of Bafoussam. Political borders are shown by black dotted lines. [Colour figure can be viewed at [wileyonlinelibrary.com](https://onlinelibrary.wiley.com/terms-and-conditions)]



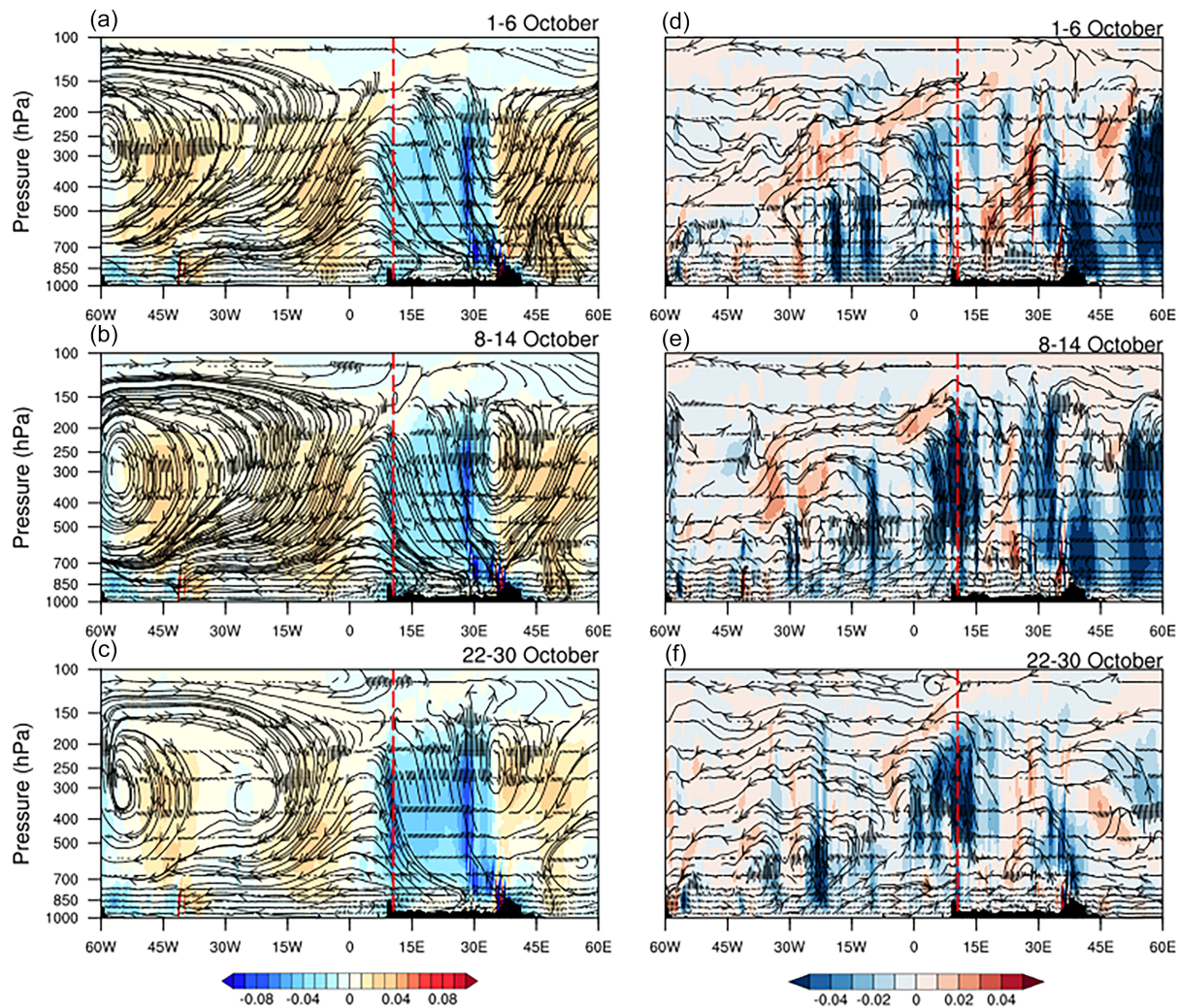


**FIGURE 8** Zonal cross sections averaged between  $5^{\circ}\text{S}$  and  $5^{\circ}\text{N}$  showing the climatology (left column) and anomalies (right column) of vertical velocity (shaded:  $\omega$  in  $\text{Pa}\cdot\text{s}^{-1}$ ) and streamlines ( $\omega$ ,  $u$ -wind in  $\text{m}\cdot\text{s}^{-1}$ ) during the periods of the respective wet spells. The climatology represents the multiyear (2000–2018) average across the periods of the respective wet spells. The days for which each anomaly was calculated are indicated in each panel heading. Anomalies are departures from the long-term mean. The vertical red-dashed lines indicate the longitude of Bafoussam and Dschang. Orography, indicating the African continent, is shown as a black silhouette. [Colour figure can be viewed at [wileyonlinelibrary.com](https://onlinelibrary.wiley.com/doi/10.1002/qj.70066)]

wave activity was overall weak. The only notable signal is an eastward-propagating Kelvin wave that passed over the study area on 14 October, that is, at the end of the second wet spell. While sporadic signals of westward-propagating TD are evident around 23 October, they do not belong to AEWs over the study area (not shown).

### 3.4 | Termination of the wet spell by an early-season cold surge

The end of October and beginning of November 2019 marked a sudden halt in the wetness across equatorial west and central Africa (see Figure 2b). The previous sections proposed the importance of a strong, anomalously northeastward-shifted SHL for the preservation of favourable conditions for recurring wet periods over the

Cameroon Highlands. Here, the MSLP anomaly field for the third wet spell features a considerably weaker SHL and a cold anomaly extending from Egypt (see Figure 7f). The following section explores dynamical mechanisms that likely initiated the end of the wet period.

Through latitude-based Hovmöllers, zonally averaged between  $28^{\circ}\text{E}$  and  $32^{\circ}\text{E}$ , that is, the band of the aforementioned cold anomaly, Figure 10 provides an overview of the temporal development of  $t_{2m}$ , temperature and meridional wind at 850 hPa ( $t_{850}$ ,  $v_{850}$ ), and geopotential height at 200 hPa ( $z_{200}$ ) over the last 10 days of October 2019. Both  $t_{2m}$  and  $t_{850}$  highlight the gradual degradation of the SHL and the southward intrusion of colder air masses (Figure 10a,b). The southernmost extent of low  $t_{2m}$  and  $t_{850}$  occurred around 26–29 October. The thick black contour denotes the 1220 geopotential

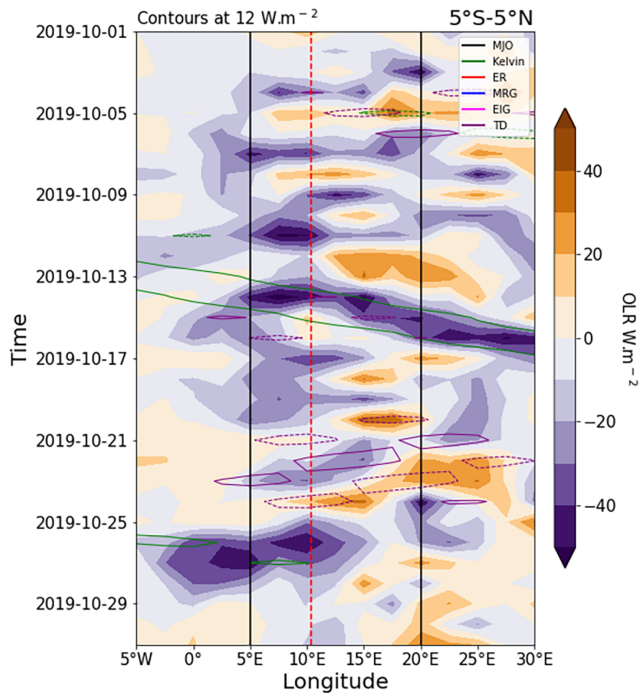


**FIGURE 9** Time–longitude (Hovmöller) section of outgoing longwave radiation (OLR;  $\text{W}\cdot\text{m}^{-2}$ ) anomaly products averaged from  $5^{\circ}\text{S}$  to  $5^{\circ}\text{N}$ . Shaded are mean anomalies calculated by subtracting the climatological mean and smoothed seasonal cycle from the total field, where the mean and seasonal cycle were based on the 2000–2018 period. Contoured are the anomalies calculated by filtering the total OLR for the specific regions of the wavenumber–frequency domain (Madden–Julian Oscillation [MJO], Kelvin waves, equatorial Rossby waves [ER], mixed Rossby–gravity waves [MRG], inertio–gravity waves [EIG], tropical disturbances [TD]). [Colour figure can be viewed at [wileyonlinelibrary.com](https://onlinelibrary.wiley.com)]

decameter (gpdm) reference isohypse at 200 hPa and shows a bulge down to around  $27^{\circ}\text{N}$  between 23 and 24 October (see also Figure 10d). As seen later in more detail, this is related to the approach of an extratropical upper-level trough over the Mediterranean. Here, the slight phase shift between the upper-level geopotential and the temperature fields hints towards baroclinic processes and thus extratropical interaction. An implication of the latter is enhanced northerlies over Sudan that set in during the passage of the trough on 24 October (Figure 10c). By 26 October, the northerlies stretch from the Mediterranean at  $35^{\circ}\text{N}$  down south to  $10^{\circ}\text{N}$ , emphasizing the extensive ventilation of cooler air towards the central Sahel. Furthermore, it is seen that the regime of southerlies in a band between  $6^{\circ}\text{N}$  and  $10^{\circ}\text{N}$ , indicative of the deep inland propagation of moist southwesterlies outlined in the previous sections, is entirely replaced by northerlies after 25 October.

Daily averaged maps of the 200-hPa geopotential in Figure 11 display the development of the upper-level

dynamics throughout the third wet spell. On 20 October, a meridionally elongated trough approached western Europe and the Mediterranean and began to impact the upper levels over northern Africa (Figure 11a). At that time, the eastern Sahel exhibited a distinct upper-level anticyclone which is related to the SHL. By 26 October, the period of maximum cold air intrusion at low levels, a cut-off low developed from the trough (Figure 11b). While it migrated slightly southward over the next few days, it barely propagated to the east and remained quasi-stationary over western Libya (Figure 11c). At the same time, an upper-level ridge prevailed over eastern Libya and Egypt. Until the dissolution of this upper-level configuration on 31 October (Figure 11d), the central Sahel was under the extratropical influence on the downstream side of the upper-level trough axis.

The impact of the upper-level developments on the low-level flow at 850 hPa is shown in Figure 12. The approach of the upper-level cut-off low led to a development of a shallow cyclone over western Libya, but more importantly to the amplification of an already existing low-level anticyclone over southeastern Europe and the central Mediterranean (cf. Figure 12a,b) which further extended over northern Africa by 28 October (Figure 12c). Along the entire eastern flank of that anticyclone, a ‘conveyor belt’ of relatively cool northerlies was established, which eroded the SHL. Eventually, the northerlies turn to northeasterlies at the southern flank of the anticyclone, penetrating into the study region of the Cameroon Highlands as dry northeasterlies (Figure 12c,d). Facilitating strong MFC together with the moist southwesterlies, the arrival of these northeasterlies in the study region coincides with the highest daily rainfall amount at the station of Bafoussam on 28 October (see Figure 2a). As elucidated in previous sections, strong MFC for intense rainfall is likely generated by converging southwesterlies controlled by a cyclone over West Africa (see cyclonic imprint in the 850-hPa wind field in Figure 12b,c) and easterlies from central Africa, which, near the end of this third wet spell, were enhanced through extratropical interaction. Eventually, the end of the third wet spell over the Cameroon Highlands, and the wet period across western and central equatorial Africa in general, is marked by a transition to an entirely easterly regime at low levels (Figure 12d) as well as the dissipation of the SHL anomaly.

## 4 | SUMMARY AND CONCLUSION

In October 2019, the city of Bafoussam in the Cameroon Highlands experienced a catastrophic landslide related to heavy rainfall with 50 deaths (Aretouyap et al., 2021). Being embedded in an extraordinary pan-African wet



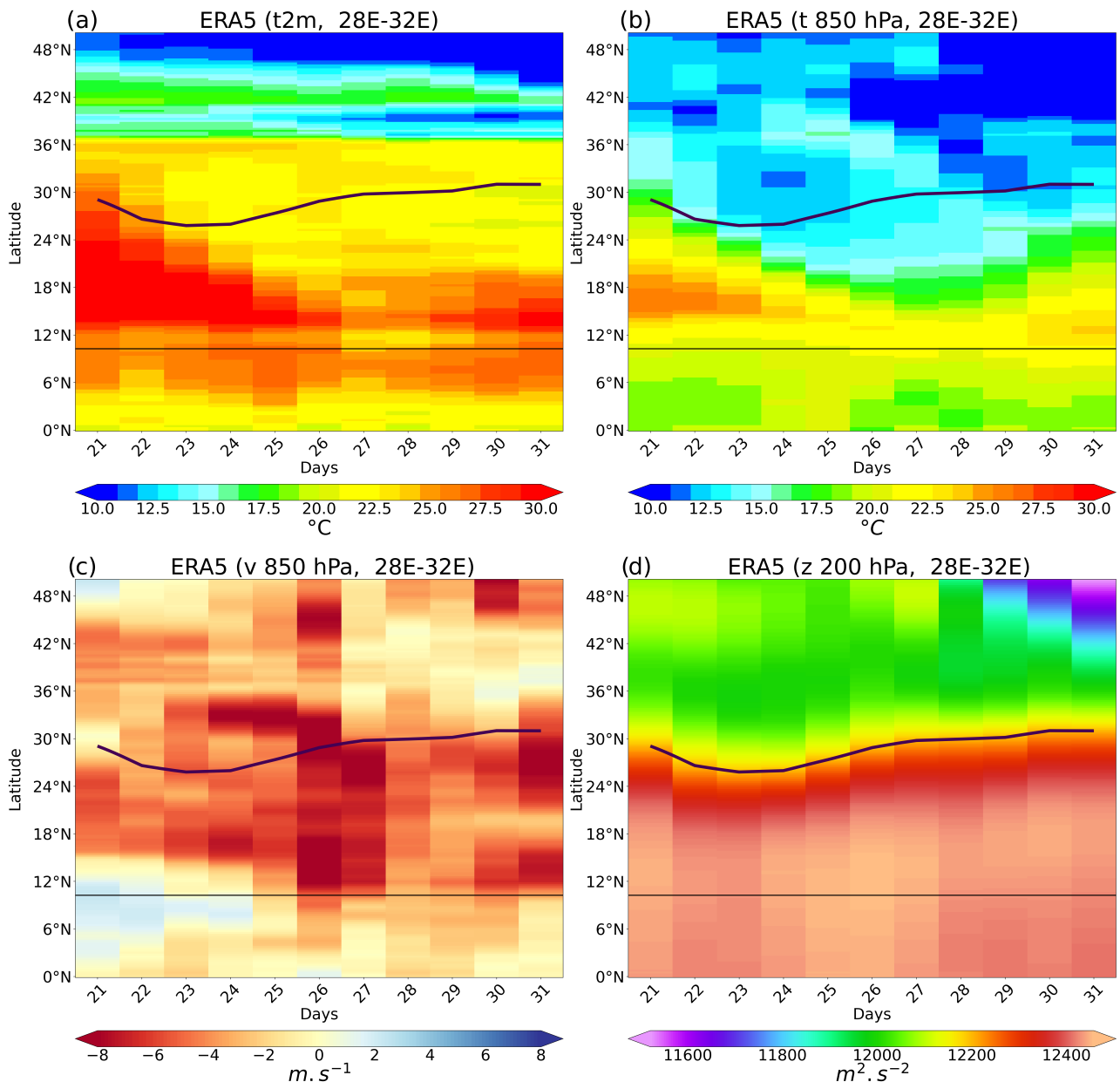


**FIGURE 10** Temporal evolution of zonally averaged (28° E–32° E) 2-m temperature (a), 850-hPa temperature (b), 850-hPa meridional wind (c) and 200-hPa geopotential height (d) from 21 to 31 October 2019. The black contour represents geopotential height at 12200 m. The horizontal black line indicates the latitude of Bafoussam and Dschang. [Colour figure can be viewed at [wileyonlinelibrary.com](https://onlinelibrary.wiley.com/terms-and-conditions)]

October–November period, which was investigated in detail by Nicholson et al. (2022) on a monthly scale, this study explored the meteorological context that facilitated this landslide event from a regional and submonthly perspective. By leveraging satellite-based data as well as historical rainfall recordings from weather stations at Bafoussam and the nearby city of Dschang, the October 2019 rainfall and its extremeness were compared against long-term reference periods. Using ERA5 data, relevant parameters such as vertically integrated moisture flux, its divergence, and 3D wind fields are examined to describe the (thermo-)dynamical drivers of three wet spells within October 2019. The main findings are:

- Based on station recordings, October 2019 was characterized by three main multiday wet spells. Three-day rainfall accumulations exceeded the respective maxima of historical data at Bafoussam and Dschang several times.
- On the regional scale, the wet spells were preconditioned by transient, westward-propagating cyclonic vortices along the Guinea coast region. Having intensified after passing the study region, these vortices facilitated effective moisture inflow from the ocean in the form of enhanced cross-equatorial southwesterlies (Lin et al., 2017; Rodwell & Hoskins, 1995). When

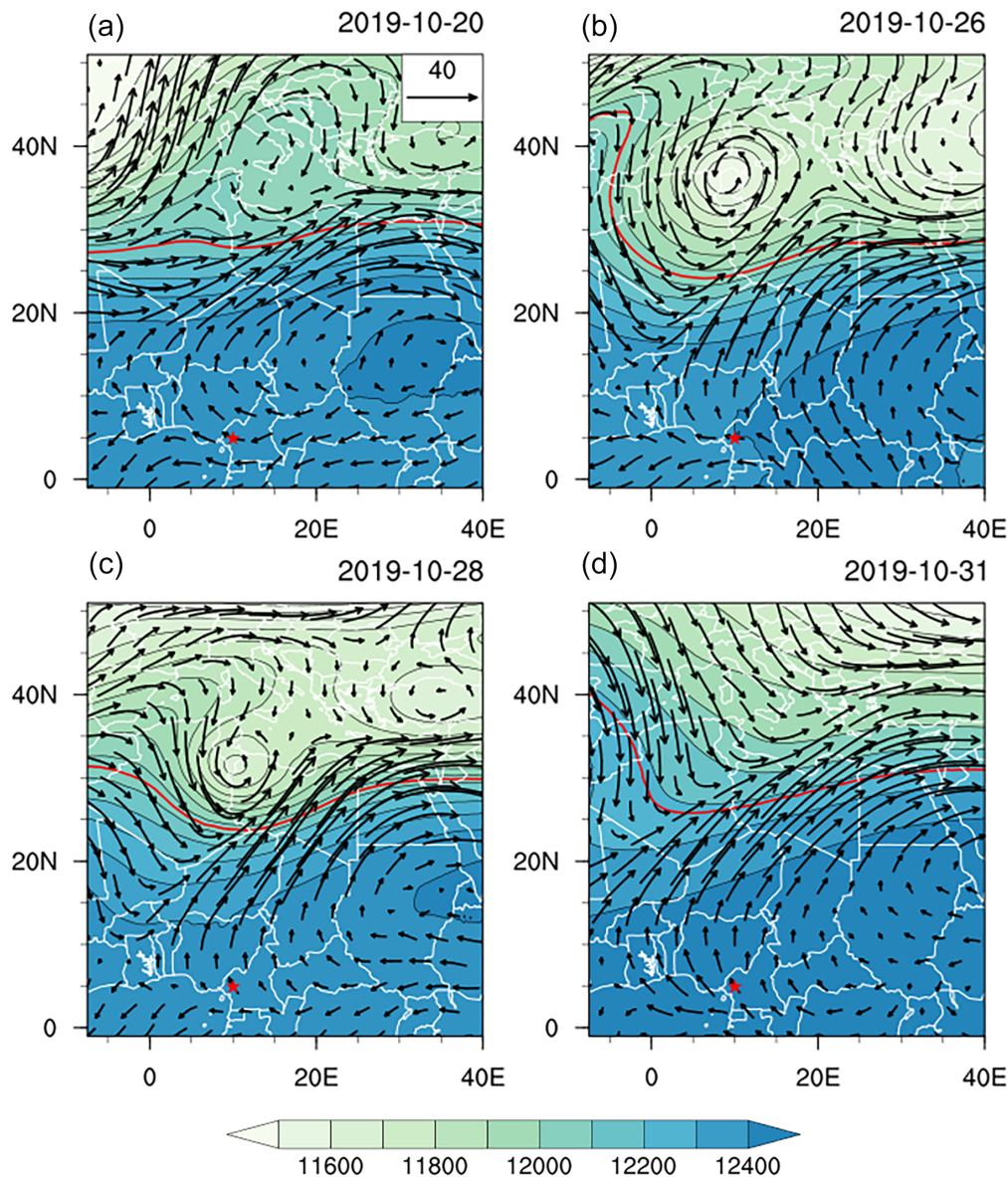


**FIGURE 11** Daily geopotential height (shaded, m) and horizontal wind (vectors,  $\text{m}\cdot\text{s}^{-1}$ ) at 200 hPa on 20, 26, 28 and 29 October 2019. The red contour identifies the value of a particular isopleth height at 12200 m. For the sake of clarity, the vectors were spaced. Country borders are represented in white. [Colour figure can be viewed at [wileyonlinelibrary.com](https://onlinelibrary.wiley.com/terms-and-conditions)]

paired with a second vortex along the equator, as seen in the second wet spell, the southwesterly moisture influx can be amplified. Strong MFC associated with intense rainfall, aside from the influence of orography, likely occurred via an interaction between these southwesterlies and prevailing easterlies from central Africa progressing westward into the study region.

- On the large scale, a strong SHL located anomalously far east and north was present, facilitating (a) a northward shift of the ITD and thus an enhancement of the inland penetration of the moist southwesterlies, and (b) a favourable environment for recurring cyclonic vortices over the Guinea coast region. Remarkably,

during October 2019, tropical wave activity was overall low and thus a negligible source for the wet-spell development.

- The rainy season of 2019 in the study region was terminated by an extratropical upper-level trough propagating across the Mediterranean Sea and northern Africa. The trough was related to an extensive cold surge from the Mediterranean into the eastern Sahara and Sahel, thereby leading to a substantial weakening of the SHL. Over the study region, this equatorward flow eventually arrived as dry northeasterlies. First, this process enhanced the rainfall by generating strong MFC together with the moist southwesterlies the day before

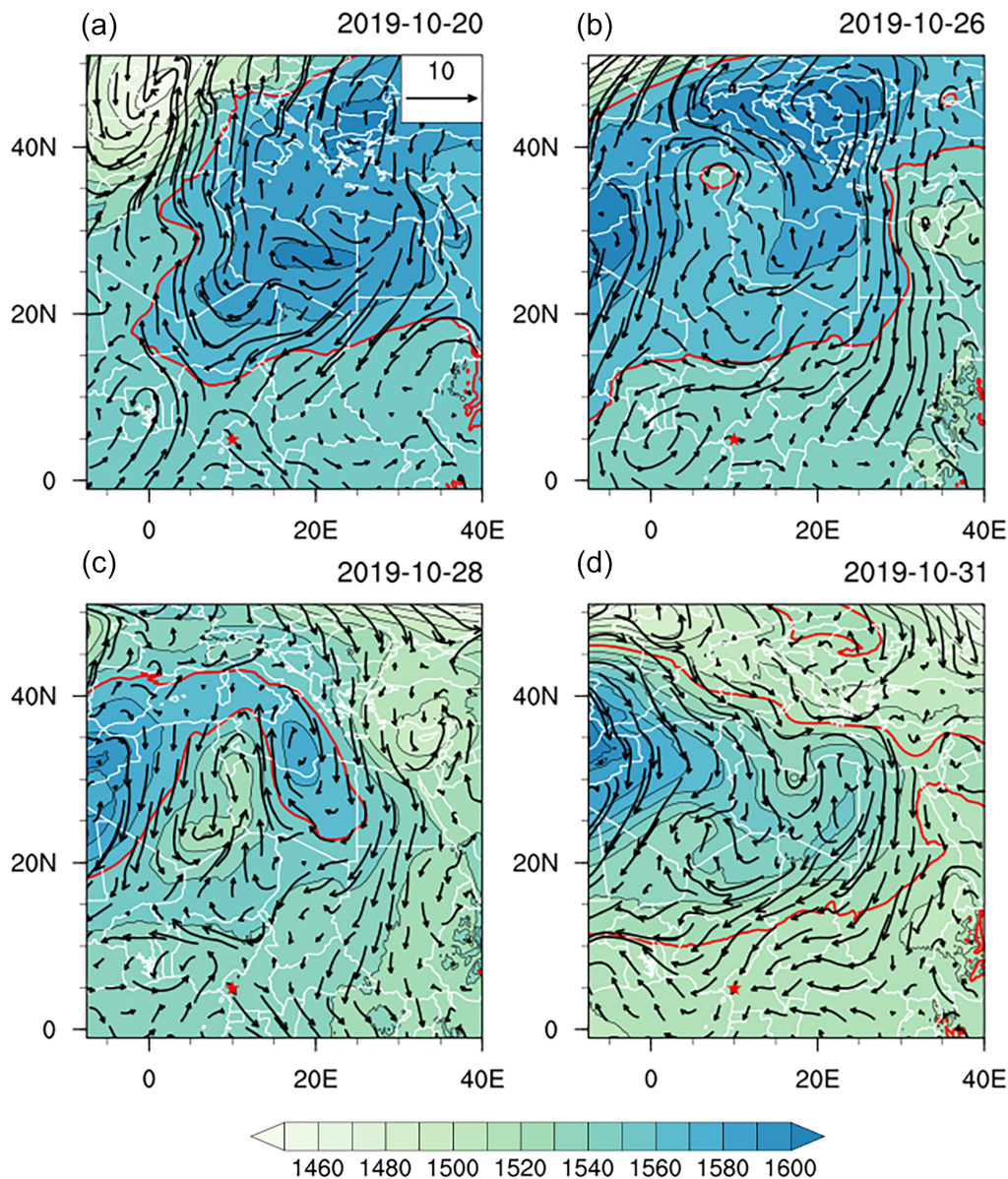


**FIGURE 12** Daily geopotential height (shaded, m) and wind (vectors,  $\text{m}\cdot\text{s}^{-1}$ ) at 850 hPa on 20, 26, 28 and 29 October 2019. The red contour identifies the value of a particular isopleth height at 1520 m. For the sake of clarity, the vectors were spaced. Country borders are represented in white. [Colour figure can be viewed at [wileyonlinelibrary.com](https://onlinelibrary.wiley.com/terms-and-conditions)]

and on 29 October 2019. After this, the arrival of dry air terminated the wet spell and ultimately the rainy season.

In this work, we have identified westward-propagating cyclonic vortices along the Guinea coast region, redirecting moisture through strong low-level southwesterlies into the study area over the Cameroon Highlands. The results showed that these vortices are particularly active during the three wet spells of October 2019. Interestingly, the relation to tropical waves is weak, if any. The existence of such westward-moving cyclonic

vortex structures over the Gulf of Guinea and southern West Africa has been documented in Knippertz et al. (2017) for June–July 2016. They were related to unusually dry and biomass-burning aerosol-laden air at stations at the Guinea coast, but very wet conditions associated with a moist low-level westerly flow farther inland. For October and in terms of their relevance for multiday rainfall periods over the Cameroon Highlands, this has not been studied in the literature so far. The origin and dynamical causes of such cyclonic vortices, sometimes occurring alongside a second equatorial vortex as couplets, and their climatological



relevance for rainfall (extremes) in the region warrant further study.

The three wet spells during October 2019 were characterized by a strong SHL. During the first and second, the SHL was located in a region between Libya, Sudan and Egypt, far from its climatological position farther west and south. This displaced SHL allowed for a more northerly location of the ITD and the AEJ during October 2019 (Nicholson et al., 2022). These authors also note a stronger Tropical Easterly Jet. According to Dunning et al. (2018), a strong SHL tends to delay the withdrawal of the West African monsoon. Overall, this suggests that the whole West African monsoon system was still in a typical state for weeks earlier, that is, in a late full-monsoon stage, and this could have allowed for the persistent development of the cyclonic vortices mentioned above. Furthermore, auxiliary analysis on sea surface temperatures for the study period (not shown) indicate states of positive IOD as well as an Atlantic Niño (Nicholson et al., 2018). To what extent they aided in maintaining the recurrence of wet spells in the study regions remains unclear and warrants further study. Finally, it is interesting to note that lower pressure over the Eastern Sahara–Sahel region has been observed during August 2020 in relation to the devastating flood in Sudan (Elagib et al., 2021) and that the recent wetting of the Sahel tends to occur in the late rainy season and away from the West Coast (Biasutti, 2019; Nicholson et al., 2018).

Previous work has shown that extratropical troughs over the Mediterranean and northern Africa are related to low-level wind and temperature fluctuations, including cold surges, over northeastern Africa both in boreal summer and winter (Vizy & Cook, 2009, 2014; Ward et al., 2021, 2023). These studies also show the time-lagged climatological impact of these tropical–extratropical interactions on rainfall within the rainbelt over northern equatorial Africa. In the present study, an autumnal cold surge related to a Mediterranean trough appeared to have weakened the east SHL such that it heralded the end of the 2019 rainy season at about 5° N in equatorial Africa. The related surge of equatorial easterlies towards Cameroon first enhanced the moisture convergence, leading to strong rainfall just before the landslide event, but then led to drier conditions when they swept over the country.

Overall, the present study highlights the intricate regional to continental-scale processes related to multiday wet spells over Cameroon in October 2019. It unravelled hitherto poorly or not understood drivers of rainfall. The intensification of rainfall and the subsequent termination of the last wet event was linked to extratropical processes, which may open the possibility to make skillful forecasts at weekly ranges (Davis et al., 2012). Our case study definitely calls for further investigations into

climatological aspects of submonthly rainfall drivers in western equatorial Africa.

## ACKNOWLEDGEMENTS


D.A. Vondou is funded by the Alexander-von-Humboldt-Stiftung as part of the Humboldt Research Fellowship for researchers of all nationalities and research areas: postdoctoral and experienced researchers programme. Andreas H. Fink and M. Maranan received funding from the BMBF grant 01LG2086A. Open Access funding enabled and organized by Projekt DEAL.

## DATA AVAILABILITY STATEMENT

The ERA5 data were obtained from the Copernicus Climate Change Service (C3S) Climate Data Store (<https://cds.climate.copernicus.eu>). IMERG data are available through the NASA earth data portal ([https://disc.gsfc.nasa.gov/datasets/GPM\\_3IMERGHH\\_06/](https://disc.gsfc.nasa.gov/datasets/GPM_3IMERGHH_06/)). The KASS-D database is operated by the Karlsruhe Institute of Technology. Rainfall data of Bafoussam and Dschang were provided by the Department of National Meteorology of Cameroon. All analyses and figures were computed and drawn using Python (<https://www.python.org/>) and NCL (<https://www.ncl.ucar.edu/>).

## ORCID

Derbetini A. Vondou  <https://orcid.org/0000-0002-8681-5328>

Marlon Maranan  <https://orcid.org/0000-0002-0324-8859>

Andreas H. Fink  <https://orcid.org/0000-0002-5840-2120>

Peter Knippertz  <https://orcid.org/0000-0001-9856-619X>

## REFERENCES

- Alber, K., Zhou, L., Roundy, P.E. & Solimine, S.L. (2023) Influence of the madden-Julian oscillation on the diurnal cycles of convection and precipitation over The Congo Basin. *Atmospheric Research*, 294, 106967. Available from: <https://doi.org/10.1016/j.atmosres.2023.106967>
- Aretouyap, Z., Kemgang, F.E.G., Domra, J.K., Bisso, D. & Njandjock, P.N. (2021) Understanding the occurrences of fault and landslide in the region of West-Cameroon using remote sensing and GIS techniques. *Natural Hazards*, 109(2), 1589–1602. Available from: <https://doi.org/10.1007/s11069-021-04890-8>
- Ayesiga, G., Holloway, C.E., Williams, C.J., Yang, G.-Y. & Ferrett, S. (2021) The observed synoptic scale precipitation relationship between Western Equatorial Africa and Eastern Equatorial Africa. *International Journal of Climatology*, 41(Suppl. 1), E582–E601. Available from: <https://doi.org/10.1002/joc.6711>
- Biasutti, M. (2019) Rainfall trends in the African Sahel: characteristics, processes, and causes. *WIREs Climate Change*, 10(4), e591. Available from: <https://doi.org/10.1002/wcc.591>
- Bulovic, N., McIntyre, N. & Johnson, F. (2020) Evaluation of IMERG V05B 30-min rainfall estimates over the high-elevation tropical Andes Mountains. *Journal of Hydrometeorology*, 21(12),

- 2875–2892. Available from: <https://doi.org/10.1175/jhm-d-20-0114.1>
- Cook, K.H. & Vizy, E.K. (2015) The Congo Basin Walker circulation: dynamics and connections to precipitation. *Climate Dynamics*, 47(3), 697–717. Available from: <https://doi.org/10.1007/s00382-015-2864-y>
- Crowhurst, D., Dadson, S., Peng, J. & Washington, R. (2020) Contrasting controls on Congo Basin evaporation at the two rainfall peaks. *Climate Dynamics*, 56(5–6), 1609–1624. Available from: <https://doi.org/10.1007/s00382-020-05547-1>
- Davis, J., Knippertz, P. & Fink, A.H. (2012) The predictability of precipitation episodes during the West African dry season. *Quarterly Journal of the Royal Meteorological Society*, 139(673), 1047–1058. Available from: <https://doi.org/10.1002/qj.2014>
- Dunning, C.M., Black, E. & Allan, R.P. (2018) Later wet seasons with more intense rainfall over Africa under future climate change. *Journal of Climate*, 31(23), 9719–9738. Available from: <https://doi.org/10.1175/jcli-d-18-0102.1>
- Elagib, N.A., Zayed, I.S.A., Saad, S.A.G., Mahmood, M.I., Basheer, M. & Fink, A.H. (2021) Debilitating floods in the Sahel are becoming frequent. *Journal of Hydrology*, 599, 126362. Available from: <https://doi.org/10.1016/j.jhydrol.2021.126362>
- Fink, A.H., Engel, T., Ermert, V., van der Linden, R., Schneidewind, M., Redl, R. et al. (2017) Mean climate and seasonal cycle. *Meteorology of Tropical West Africa*, P1–P39. Available from: <https://doi.org/10.1002/9781118391297.ch1>
- Hersbach, H., Bell, B., Berrisford, P., Hirahara, S., Horányi, A., Muñoz-Sabater, J. et al. (2020) The ERA5 global reanalysis. *Quarterly Journal of the Royal Meteorological Society*, 146(730), 1999–2049. Available from: <https://doi.org/10.1002/qj.3803>
- Huffman, G.J., Bolvin, D.T., Joyce, R., Nelkin, E.J., Tan, J., Braithwaite, D. et al. (2023) Algorithm Theoretical Basis Document (ATBD) NASA Global Precipitation Measurement (GPM) Integrated Multi-satellite Retrievals for GPM (IMERG). [https://gpm.nasa.gov/sites/default/files/2023-07/IMERG\\_V07\\_ATBD\\_final\\_230712.pdf](https://gpm.nasa.gov/sites/default/files/2023-07/IMERG_V07_ATBD_final_230712.pdf)
- Igri, P.M., Tanessong, R.S., Vondou, D.A., Panda, J., Garba, A., Mkankam, F.K. et al. (2018) Assessing the performance of WRF model in predicting high-impact weather conditions over central and Western Africa: an ensemble-based approach. *Natural Hazards*, 93(3), 1565–1587. Available from: <https://doi.org/10.1007/s11069-018-3368-y>
- Kenfack, K., Marra, F., Djomou, Z.Y., Tchotchou, L.A.D., Tamoffo, A.T. & Vondou, D.A. (2024) Dynamic and thermodynamic contribution to the October 2019 exceptional rainfall in western central Africa. *Weather and Climate Dynamics*, 5, 1457–1472. Available from: <https://doi.org/10.5194/wcd-5-1457-2024>
- Kengni, L., Mbousso, A.N., Njueya Kopa, A., Tankou, C.M., Tematio, P. & Ndam Ngoupayou, J.R. (2019) Rainfall variability on the southern slope of the Bambouto mountain (West-Cameroon) and impact on the crop cultivation calendar. *Journal of African Earth Sciences*, 154, 164–171. Available from: <https://doi.org/10.1016/j.jafrearsci.2019.03.020>
- Knippertz, P. & Fink, A.H. (2008) Dry-season precipitation in tropical West Africa and its relation to forcing from the Extratropics. *Monthly Weather Review*, 136(9), 3579–3596. Available from: <https://doi.org/10.1175/2008mwr2295.1>
- Knippertz, P., Fink, A.H., Deroubaix, A., Morris, E., Tocquer, F., Evans, M.J. et al. (2017) A meteorological and chemical overview of the DACCWA field campaign in West Africa in June–July 2016. *Atmospheric Chemistry and Physics*, 17(17), 10893–10918. Available from: <https://doi.org/10.5194/acp-17-10893-2017>
- Lafore, J.P. (2017) Deep convection. In: Parker, D.J. & Diop-Kane, M. (Eds.) *Meteorology of tropical West Africa: the forecasters' handbook*. Chichester, UK: John Wiley & Sons, pp. 161–223.
- Liebmann, B. & Smith, C.A. (1996) Description of a complete (interpolated) outgoing longwave radiation dataset. *Bulletin of the American Meteorological Society*, 77(6), 1275–1277. Available from: <https://doi.org/10.2307/26233278>
- Lin, A., Zhang, R. & He, C. (2017) The relation of cross-equatorial flow during winter and spring with South China Sea summer monsoon onset. *International Journal of Climatology*, 37, 4576–4585. Available from: <https://doi.org/10.1002/joc.5106>
- Maranan, M., Fink, A.H., Knippertz, P., Amekudzi, L.K., Atiah, W.A. & Stengel, M. (2020) A process-based validation of GPM IMERG and its sources using a mesoscale rain gauge network in the West African Forest zone. *Journal of Hydrometeorology*, 21(4), 729–749. Available from: <https://doi.org/10.1175/jhm-d-19-0257.1>
- Maranan, M., Fink, A.H., Knippertz, P., Francis, S.D., Akpo, A.B., Jegede, G. et al. (2019) Interactions between convection and a moist vortex associated with an extreme rainfall event over southern West Africa. *Monthly Weather Review*, 147(7), 2309–2328. Available from: <https://doi.org/10.1175/mwr-d-18-0396.1>
- Marc, O., Oliveira, R.A.J., Gosset, M., Emberson, R. & Malet, J.-P. (2022) Global assessment of the capability of satellite precipitation products to retrieve landslide-triggering extreme rainfall events. *Earth Interactions*, 26(1), 122–138. Available from: <https://doi.org/10.1175/ei-d-21-0022.1>
- Moihamette, F., Pokam, W.M., Diallo, I. & Washington, R. (2024) Response of regional circulation features to the Indian Ocean dipole and influence on Central Africa climate. *Climate Dynamics*, 62, 1–21. Available from: <https://doi.org/10.1007/s00382-024-07251-w>
- Molua, E. (2006) Climatic trends in Cameroon: implications for agricultural management. *Climate Research*, 30, 255–262. Available from: <https://doi.org/10.3354/cr030255>
- Mouassom, F.L. & Tamoffo, A.T. (2024) Understanding the environmental conditions of the extreme precipitation event on June 20, 2015, in the city of Douala, Cameroon. *Natural Hazards*, 120, 11527–11546. Available from: <https://doi.org/10.1007/s11069-024-06681-3>
- Moudi, P.I., Kammalac Jores, T., Talib, J., Appolinaire, V.D., Hirons, L., Christian, N. et al. (2023) Strengthening weather forecast and dissemination capabilities in Central Africa: case assessment of intense flooding in January 2020. *Climate Services*, 32, 100411. Available from: <https://doi.org/10.1016/j.cliser.2023.100411>
- Nana, H.N., Tanessong, R.S., Tchotchou, L.A.D., Tamoffo, A.T., Moihamette, F. & Vondou, D.A. (2023) Influence of strong South Atlantic Ocean dipole on the Central African rainfall's system. *Climate Dynamics*, 62(1), 1–16. Available from: <https://doi.org/10.1007/s00382-023-06892-7>
- NASA. (2023) NASA IMPORTANT: Errors in GPROF Orbits within Select (2023). IMERG Final Data Products [WWW Document]. URL <https://gpm.nasa.gov/data/news/important-errors-gprof-orbits-within-select-imerg-final-data-products>
- Nicholson, S.E., Fink, A.H. & Funk, C. (2018) Assessing recovery and change in West Africa's rainfall regime from a 161-year record. *International Journal of Climatology*, 38(10), 3770–3786. Available from: <https://doi.org/10.1002/joc.5530>

- Nicholson, S.E., Fink, A.H., Funk, C., Klotter, D.A. & Satheesh, A.R. (2022) Meteorological causes of the catastrophic rains of October/November 2019 in equatorial Africa. *Global and Planetary Change*, 208, 103687. Available from: <https://doi.org/10.1016/j.gloplacha.2021.103687>
- Osei, M.A., Aryee, J.N.A., Agyekum, J., Ashong, J., Ansah, S.O., Ahiataku, M.A. et al. (2023) Environment of severe storm formations over West Africa on the 26–28 June 2018. *Meteorological Applications*, 30(1), e2109. Available from: <https://doi.org/10.1002/met.2109>
- Osei, M.A., Padi, M., Yahaya, B., Baidu, M., Quansah, E., Aryee, J.N.A. et al. (2022) The dynamics of dry and wet monsoon MCS formation over West Africa: case assessment of February 13, 2018 and June 18, 2018. *Quarterly Journal of the Royal Meteorological Society*, 149(750), 133–151. Available from: <https://doi.org/10.1002/qj.4399>
- Peyrillé, P., Roehrig, R. & Sanogo, S. (2023) Tropical waves are key drivers of extreme precipitation events in the Central Sahel. *Geophysical Research Letters*, 50, e2023GL103715. Available from: <https://doi.org/10.1029/2023GL103715>
- Pokam, W.M., Djotang, L.A.T. & Mkankam, F.K. (2011) Atmospheric water vapor transport and recycling in equatorial Central Africa through NCEP/NCAR reanalysis data. *Climate Dynamics*, 38(9–10), 1715–1729. Available from: <https://doi.org/10.1007/s00382-011-1242-7>
- Rodwell, M. & Hoskins, B. (1995) A model of the Asian summer monsoon part II: cross-equatorial flow and PV behavior. *Journal of the Atmospheric Sciences*, 52, 1341–1356. Available from: [https://doi.org/10.1175/1520-0469\(1995\)052<1341:amotas>2.0.co;2](https://doi.org/10.1175/1520-0469(1995)052<1341:amotas>2.0.co;2)
- Schlueter, A., Fink, A.H., Knippertz, P. & Vogel, P. (2019) A systematic comparison of tropical waves over northern Africa. Part I: influence on rainfall. *Journal of Climate*, 32(5), 1501–1523. Available from: <https://doi.org/10.1175/jcli-d-18-0173.1>
- Sinclair, Z., Lenouo, A., Tchawoua, C. & Janicot, S. (2015) Synoptic kelvin type perturbation waves over Congo basin over the period 1979–2010. *Journal of Atmospheric and Solar-Terrestrial Physics*, 130, 43–56. Available from: <https://doi.org/10.1016/j.jastp.2015.04.015>
- Tamoffo, A.T., Amekudzi, L.K., Weber, T., Vondou, D.A., Yamba, E.I. & Jacob, D. (2022) Mechanisms of rainfall biases in two CORDEX-CORE regional climate models at rainfall peaks over central equatorial Africa. *Journal of Climate*, 35(2), 639–668. Available from: <https://doi.org/10.1175/jcli-d-21-0487.1>
- Tan, J., Petersen, W.A. & Tokay, A. (2016) A novel approach to identify sources of errors in IMERG for GPM ground validation. *Journal of Hydrometeorology*, 17(9), 2477–2491. Available from: <https://doi.org/10.1175/jhm-d-16-0079.1>
- Tan, J., Huffman, G.J., Bolvin, D.T., Nelkin, E.J. & Rajagopal, M. (2021) SHARPEN: a scheme to restore the distribution of averaged precipitation Fields. *Journal of Hydrometeorology*, 22(8), 2105–2116. Available from: <https://doi.org/10.1175/JHM-D-20-0225.1>
- Tozer, B., Sandwell, D.T., Smith, W.H.F., Olson, C., Beale, J.R. & Wesel, P. (2019) Global bathymetry and topography at 15 arc sec: SRTM15+. *Earth and Space Science*, 6(10), 1847–1864. Available from: <https://doi.org/10.1029/2019ea000658>
- Vallès-Casanova, I., Lee, S.-K., Foltz, G.R. & Pelegrí, J.L. (2020) On the spatiotemporal diversity of Atlantic Niño and associated rainfall variability over West Africa and South America. *Geophysical Research Letters*, 47, e2020GL087108. Available from: <https://doi.org/10.1029/2020GL087108>
- Vizy, E.K. & Cook, K.H. (2009) A mechanism for African monsoon breaks: Mediterranean cold air surges. *Journal of Geophysical Research*, 114, D01104. Available from: <https://doi.org/10.1029/2008JD010654>
- Vizy, E.K. & Cook, K.H. (2014) Impact of cold air surges on rainfall variability in the Sahel and wet African tropics: a multi-scale analysis. *Climate Dynamics*, 43, 1057–1081. Available from: <https://doi.org/10.1007/s00382-013-1953-z>
- Vogel, P., Knippertz, P., Fink, A.H., Schlueter, A. & Gneiting, T. (2018) Skill of global raw and postprocessed ensemble predictions of rainfall over northern tropical Africa. *Weather and Forecasting*, 33(2), 369–388. Available from: <https://doi.org/10.1175/waf-d-17-0127.1>
- Ward, N., Fink, A.H., Keane, R.J., Guichard, F., Marsham, J.H., Parker, D.J. et al. (2021) Synoptic timescale linkage between mid-latitude winter troughs Sahara temperature patterns and northern Congo rainfall: a building block of regional climate variability. *International Journal of Climatology*, 41(5), 3153–3173. Available from: <https://doi.org/10.1002/joc.7011>
- Ward, N., Fink, A.H., Keane, R.J. & Parker, D.J. (2023) Upper-level midlatitude troughs in boreal winter have an amplified low-latitude linkage over Africa. *Atmospheric Science Letters*, 24(1), e1129. Available from: <https://doi.org/10.1002/asl.1129>
- Wamba Tchinda, C., Tchakoutio Sandjon, A., Djotang Tchotchou, A.L., Siwe, A.N. & Vondou, D. (2023) The influence of intraseasonal oscillations on rainfall variability over Central Africa: case of the 25–70 days variability. *Scientific Reports*, 13, 19842. Available from: <https://doi.org/10.1038/s41598-023-46346-y>
- Wheeler, M. & Kiladis, G.N. (1999) Convectively Coupled Equatorial Waves: Analysis of Clouds and Temperature in the Wavenumber–Frequency Domain. *Journal of the Atmospheric Sciences*, 56(3), 374–399. Available from: [https://doi.org/10.1175/1520-0469\(1999\)056<0374:CCEWAO>2.0.CO;2](https://doi.org/10.1175/1520-0469(1999)056<0374:CCEWAO>2.0.CO;2)
- World Population Review 2024. <https://worldpopulationreview.com/continents/sub-saharan-africa-population>
- Zangmene, F.L., Ngapna, M.N., Ateba, M.C.B., Mboudou, G.M.M., Defo, P.L.W., Kouo, R.T. et al. (2023) Landslide susceptibility zonation using the analytical hierarchy process (AHP) in the Bafoussam-Dschang region (West Cameroon). *Advances in Space Research*, 71(12), 5282–5301. Available from: <https://doi.org/10.1016/j.asr.2023.02.014>
- Zebaze, S., Lenouo, A., Tchawoua, C., Gaye, A.T. & Kamba, F.M. (2017) Interaction between moisture transport and Kelvin waves events over Equatorial Africa through ERA-interim. *Atmospheric Science Letters*, 18(7), 300–306. Available from: <https://doi.org/10.1002/asl.756>

**How to cite this article:** Vondou, D.A., Maranan, M., Fink, A.H. & Knippertz, P. (2025) Meteorological conditions leading to a catastrophic, rain-induced landslide in Cameroon in October 2019. *Quarterly Journal of the Royal Meteorological Society*, e70066. Available from: <https://doi.org/10.1002/qj.70066>